

# Working Strategies for Addressing Microzoning Studies in Urban Areas: Lessons from the 2009 L'Aquila Earthquake

Giovanna Vessia, Mario Luigi Rainone and Patrizio Signanini

## 1 Introduction

The Italian territory is affected by frequent seismic events producing high intensity in near-field areas. Although the maxima moment magnitudes are about 7, several disasters were associated with historical strong earthquakes. Hence, the seismic effects in Italy “can be considered as historical variables of the degree of intensity: historical building techniques, economic levels and population size” (Guidoboni and Ferrari 2000). Many are the historical documents collected by local authorities and the Church since the Middle Age (among others Baratta 1901; Guidoboni et al. 2007) that systematically witness the consequences of the past earthquakes in terms of fatalities, disruptions in urban centers and sometimes the economic losses. Recently, Guidoboni et al. (2007) collected all this information in a Catalogue of strong earthquakes in Italy from 461B.C. to 2000. This catalogue shows that catastrophic seismic events occur every  $5\frac{1}{2}$  year, on average, from the Middle Age up to now: 4509 sites were hurt by seismic events causing Intensity degrees higher than VII (MCS scale) (Guidoboni 2013), whereas over the whole Italian territory 11,440 sites suffered heavy damages and 4800 victims. Some crossed analyses on economic and social effects of Italian earthquakes suggested that after strong seismic events, the affected human communities suffered economic crises (Guidoboni et al. 2011). For instance, the seismic event that occurred at Ferrara city in 1570 (Guidoboni and Comastri 2005) destroyed many palaces and towers boosting the first “Seismic Building code” written by the famous architect Pirro

---

G. Vessia (✉) · M.L. Rainone · P. Signanini  
Department of Engineering and Geology, University “G. D’Annunzio”  
of Chieti-Pescara, Chieti, Italy  
e-mail: g.vessia@unich.it

G. Vessia  
Institute of Research for Hydrogeological Protection, National Research Council  
(CNR-IRPI), Bari, Italy

Ligorio (ed. Guidoboni 2006). In addition, five great events known as 1783 Calabrian earthquakes and 1908 Messina earthquake caused 80,000 fatalities on both sides of Reggio Calabria and Messina plus a tsunami wave. This latter event definitively changed the face of Messina city and produced a long lasting economic crisis (Guidoboni 2013).

In recent years, the Department of Civil Protection estimated the economic losses due to the strong earthquakes that occurred in Italy from 1968 to 2003 (Fig. 1). It is worth noticing that these losses rapidly increase over time maybe because of the rapid urbanization of several portions of the territory where the methods used to estimate the seismic hazard and risk were not effective at all. The urgent need to improve the methods used for determining seismic hazard and risk assessments is supported by a recent event: the April 6, 2009 L'Aquila earthquake (Equivalent Moment Magnitude  $M_w = 6.3$ ). It is the third largest event recorded by the Italian accelerometer seismic network after the Friuli earthquake in 1976 ( $M_w = 6.4$ ) and the Irpinia earthquake in 1980 ( $M_w = 6.9$ ). It can be considered one of the most mournful seismic event occurred in recent time in Italy: 308 fatalities, 60.000 people displaced (data source <http://www.protezionecivile.it>) and estimated damages for 1894 ME (data source <http://www.ngdc.noaa.gov>). Nonetheless, the signals recorded by the fixed and temporary seismic stations represent a valuable source of information for earthquake scientists to test the knowledge about the near field (the directivity, high frequency content and high vertical components of the propagated seismic waves) and local amplification effects studied so far.

Forty years ago, the 1976 Friuli earthquake boosted quantitative microzoning studies associated with the macroseismic maps of damages where differential local site effects in near-field conditions were highlighted. Subsequently, after the 1980 Irpinia earthquake, the project "Geodinamica" was financed: it was the first research project, in Italy, that tried to introduce numerical one- and two-dimensional (1D and 2D) finite element simulations to assess site effects (Postpischl et al. 1985). Then, after the Umbria-Marche earthquake in 1997 ( $M_w = 5.9$ ), some evidences of local seismic effects (e.g. Nocera Umbra case study), due to both seismic impedance contrasts between neighbor geological formations and their surface and subsurface geometric shapes, suggested to deal with microzoning studies in order to reduce the costs of strong Italian earthquakes in terms of structural damages and economic

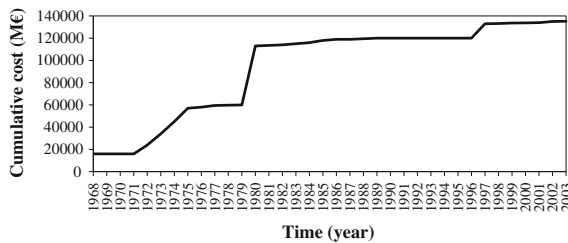


**Fig. 1** Cumulative losses due to the strong earthquakes in Italy from 1968 to 2003 (in M€) (after Guidoboni et al. 2013 modified)

losses. Later on, the National Working Group against Earthquakes (GNDT), within the framework of the project “ProgettoEsecutivo 1998”, undertook novel studies on probabilistic national seismic hazard (Galadini et al. 2000) and on microzonation (Marcellini 1999). The 2002 Molise earthquake ( $M_w = 5.7$ ) highlighted the need of an up-to-date technical code for designing structures and infrastructures against earthquakes as well as an up-to-date national reference map of seismic hazard. Hence, the first edition of the New Italian Building Codes was published in 2003 by the issue of the Decree of the President of the Council of Ministers (DPCM) 3274. It implemented by law the New Italian Seismic Hazard Map calculated for a return period of 475 years. In 2008, by means of the issue of the Ministerial Decree (DM 14 gennaio 2008), the new technical provisions became law after several revisions were implemented from their first issue on 2003. At the same time, the Italian Department of Civil Protection (DPC) published in 2008 the “national guidelines for executing microzoning studies” (Gruppo di Lavoro 2008) related to liquefaction, instability and amplification phenomena. The working scales vary between 1:5000 and 1:10,000 depending on the size of the municipal territory. Such activities can be performed at three detail levels: level 1, by mapping homogeneous geological units with respect to seismic behavior; level 2, by mapping numerical indexes for homogeneous susceptible areas; level 3, by mapping homogeneous seismic responses carried out by means of 1D, 2D and even three-dimensional (3D) numerical analyses. The L’Aquila earthquake of 2009 occurred when the discussion on the best techniques for both measuring the seismic properties at the site and representing seismic hazard scenarios at selected return periods was at its apex. Soon after the terrible unpredicted main shock on April 6th, 2009, all the financial efforts of the Italian government were devoted on one hand to face the emergency, and, on the other hand, to check the effectiveness of the technical guidelines already published. Many strong and weak motion records were available for the main shock and its strong and weak after shocks. These records are now published on two public databases: ITACA (for strong motion events) at [http://itaca.mi.ingv.it/ItacaNet/itaca10\\_links.htm](http://itaca.mi.ingv.it/ItacaNet/itaca10_links.htm) and ISIDE (for weak motion and instrumental events) <http://iside.rm.ingv.it/iside/standard/index.jsp> managed by the Italian National Institute of Geophysics and Volcanology (INGV). In addition, all the microzonation studies undertaken in the most damaged areas of the Aterno Valley have been collected in a book published in 2010 (Working Group MS-AQ 2010). It aimed at providing microzonation maps in terms of amplification factors for reconstruction purposes. Twelve macro areas within the Aterno Valley that experienced higher than the VI degree of seismic intensity measured on the Mercalli-Cancani-Sieberg (MCS) scale (Fig. 2) were chosen for the microzonation. The present study focuses on microzoning studies addressing the Aterno Valley after the 2009 L’Aquila earthquake. The authors discuss the role played by geo-lithological conditions in the amplification effects occurred at different sections of the Aterno Valley and the most efficient techniques to investigate them. Moreover, the authors provide suggestions to quantify surface geology contribution to the overall amplification effects in near-field conditions by means of 1D and 2D numerical simulations. Furthermore, different aspects of the Italian strategy to tackle microzoning studies are discussed by

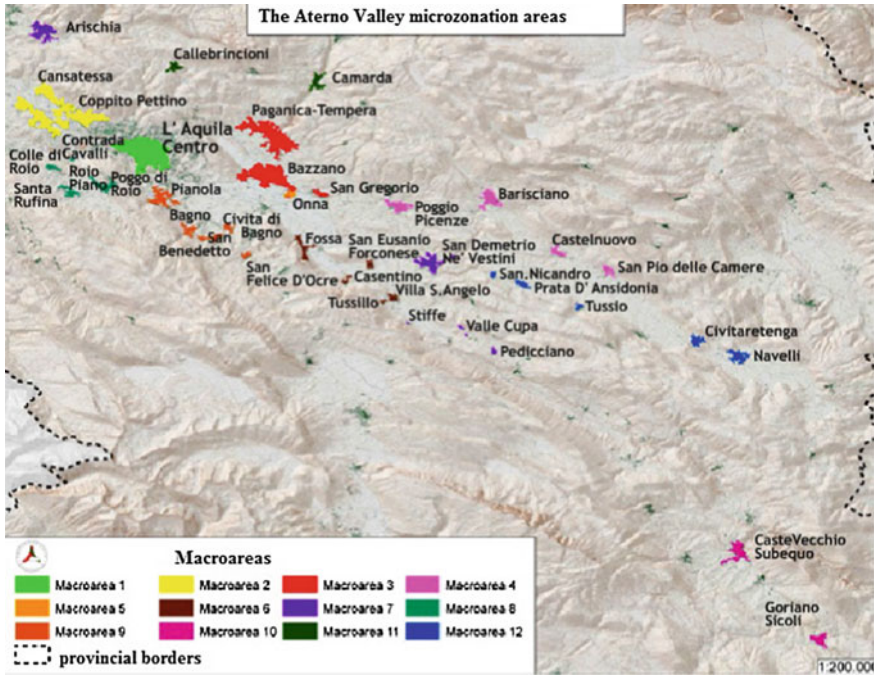


Fig. 2 Twelve macroareas map where microzoning activities have been performed

means of seismic monitoring activities and noise measurements that are carried on in five macroareas of the Aterno Valley, that are the Macroarea 1 (L'Aquila city center), Macroarea 5 (Onna city), Macroarea 6 (Villa Sant'Angelo-Tussillo), Macroarea 7 (Arischia) and Macroarea 8 (Poggio di Roio) (Fig. 2).

Accordingly, after the Introductory Sects. 1, 2 briefly describes the features of the recent and historical seismicity of L'Aquila and Onna; Sect. 3 outlines the surface geology of the Aterno Valley. In particular, litho-technical descriptions of the first 30 m under the five seismic stations that recorded the main shock on April 6th are reported. Section 4 presents the results of the seismic monitoring performed between April and July 2009 in 5 sites of the Aterno Valley (Onna, Arischia, Villa Sant'Angelo, Tussillo, Poggio di Roio and L'Aquila city). These measures are discussed with respect to the microzoning maps drawn at the corresponding macroareas in terms of amplification factors. Section 5 collects the authors' experiences on numerical simulations of local amplification phenomena—in free-field conditions occurred in two parts of the Aterno Valley: 1D analyses performed at L'Aquila city center and 2D analyses along the Monticchio-Onna-San Gregorio alignment. Finally, Sect. 6 presents noise measures recorded at Villa Sant'Angelo and Tussillo sites and four seismic stations (near L'Aquila city). The latter are used to derive the natural frequencies at the sites through the Nakamura H/V ratios calculated for both weak motions after the 2009 L'Aquila earthquake and the noise measures recorded some days after the main shock.

## 2 Main Features of the Aterno Valley Seismicity

The Aterno Valley is an intermountain quaternary basin generated by the normal fault tectonic regime within the central sector of the Apennine chain. It is located between the Gran Sasso Mountain and the Monti Ocre-Velino-Sirente structural units. The Aterno Valley is elongated NW-SE and it can be subdivided into three areas: northern, southern and central area where L'Aquila city is located. Before the 2009 L'Aquila earthquake, no active faults had been identified within the Aterno Valley according to the Database of Individual Seismogenic Sources DISS3 (DISS Working group 2009), that is a geo-referenced repository of seismogenic source models for Italy. Nonetheless, Meletti and Valensise (2004) included the Paganica Fault (responsible for the 2009 L'Aquila earthquake) within the inventory of the active faults belonging to the central sector of the Apennine chain. On the 6th of April, 2009, at 01:32 UTC, a  $MW = 6.3$  earthquake struck the Aterno Valley, especially L'Aquila city center and its surroundings causing 306 fatalities and the displacement of more than 60,000 people, due to the heavy damages to civil structures and buildings. Moreover, a large part of the historical buildings and churches were severely affected: the old town of L'Aquila was strongly damaged and Onna city (Fig. 3), South of L'Aquila, was fully destroyed. The MCS intensity reached IX-X degree at the Onna site and L'Aquila city center. The main shock followed a seismic sequence that had started in October 2008 and was followed by thousands of aftershocks. The aftershock distribution (Chiarabba et al. 2009), as well as DinSAR analyses (Atzori et al. 2009) in Fig. 4a, showed the reactivation of Paganica fault, 15 km long, NW-SE striking (about  $150^\circ$ ) and SW dipping structure (about  $50^\circ$ ). The fault plane was 28 and 17.5 km wide and the hypocenter was located at 9.5 km (Ciriella et al. 2009). Furthermore, the joint inversion of SAR interferometric and GPS data performed by Atzori et al. (2009), Fig. 4b, showed an asymmetric deformation field with maximum displacements no greater than 10–12 cm, compared to a maximum slip of about 1 m recognized SE of L'Aquila town. Accordingly, Milana et al. (2011) recognized a decreasing trend in the amplification factors from South to North. Such behavior suggested a relevant role of the fault directivity effects (Atzori et al. 2009).



**Fig. 3** Onna city after the April 6, 2009 seismic event struck (a, b); L'Aquila city (c)



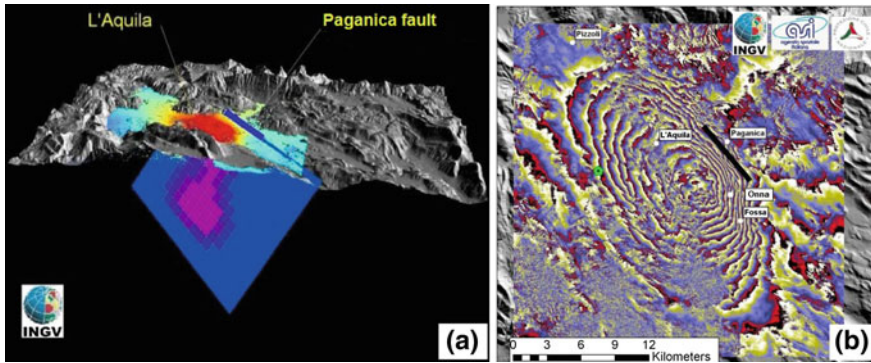


**Fig. 4** **a** Fault plane solution by InSAR data inversion, corresponding to the theory of a seismogenic and capable Paganica fault (Salvi et al. 2009); **b** COSMO-SkyMed ascending interferogram (post-event image April 13), normal baseline 430 m, look angle  $36^\circ$  from an ascending orbit. *Green symbol* indicates the  $M_w = 6.3$  main shock location (INGV 2009)

Looking at Fig. 4b, each concentric fringe quantifies 1.5 cm of co-seismic vertical deformation; in addition, Onna is placed where the settlement lines are denser while L'Aquila city shows lower vertical displacement. As can be seen, Onna city is less than 5 km far from the Paganica fault, whereas L'Aquila city is 5.7 km far from it: the two cities fall within the Paganica fault hanging wall. Unfortunately, main shock registrations are only available at L'Aquila city center and in the northern part of the Aterno Valley. Nonetheless, Onna seems to have experienced higher regime of vertical deformation than L'Aquila city. Does it depend on its vicinity to the Paganica fault or could it be due to the deformability of the sediments where Onna is settled? In the following, some clues will be collected to show the prominent role of sediments on the damages occurred at Onna and L'Aquila. Finally, it is worth noticing that the epicentral projection of the hypocenter area (see Fig. 4b, the green point) doesn't correspond to the most solicited area. Thus, hereafter, the epicentral distance of seismic stations will not be taken into consideration. Instead, the intensity values drawn from a Macroseismic map (Fig. 5) will be taken as the reference for the following microzoning studies.

Considering the historical seismicity of Onna (Table 1) and L'Aquila (Table 2) there are only four seismic events that heavily struck both cities: two out of four had Intensities as high as 9 MCS. Baratta (1901) collected documentary information on the most ancient seismic events at Onda (the ancient name of Onna): in 1461 and 1703 he reported two strong earthquakes that caused several deaths and a complete destruction of buildings at Onda. Baratta plotted the boundaries of the major damaged areas due to some historical seismic events that affected the southern part of the Aterno River Valley. Figure 6 shows the elliptical boundary of the 1703 earthquake centered at L'Aquila city. As reported by the author, this event was characterized by several shocks with major damage registered South-eastward of L'Aquila city. Thus, it seems to be an historically based idea that, as observed after 2009 L'Aquila earthquake, the damage features can be associated with amplified

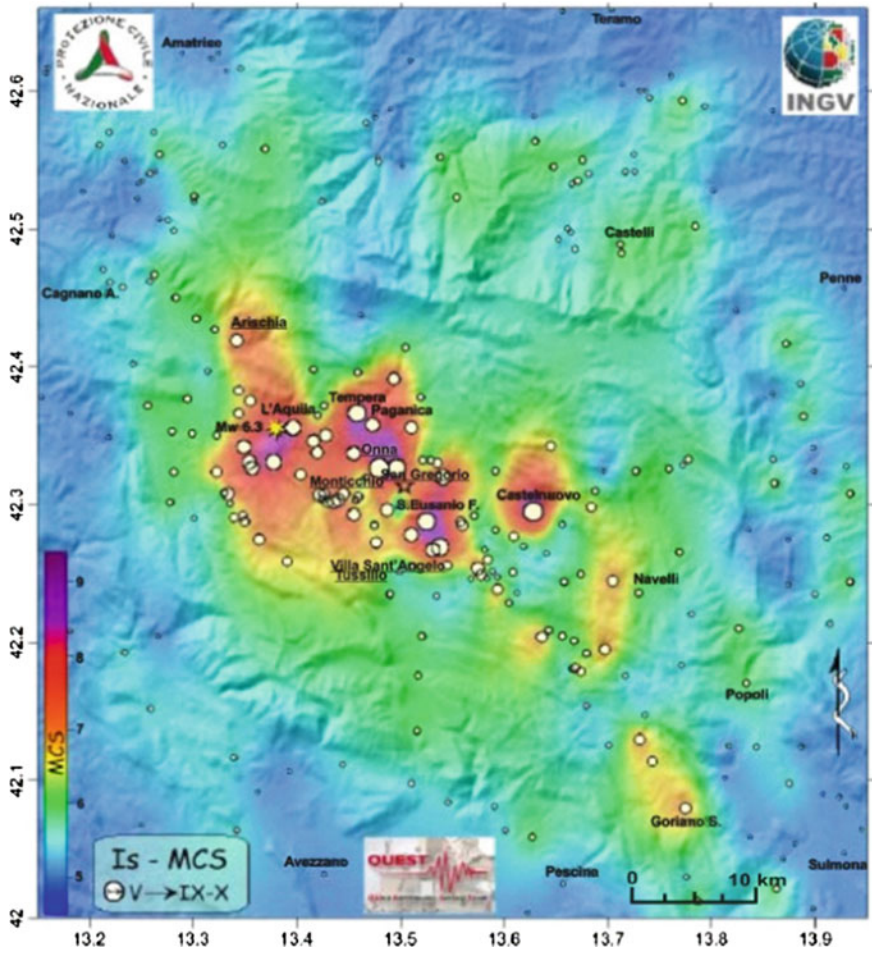


Fig. 5 Macroseismic map of the main shock on April 6, 2009 (Galli and Camassi 2009 modified)

Table 1 Historical seismicity at Onna

Intensity at the Onna site (MCS)	Year/month/day/hour	Epicentral area	Intensity at the epicentral site (MCS)	Magnitude moment (Mw)
7-8	1915/01/13/06:52	Avezzano	11	6.99
7-8	1958/06/24/06:07	Aquilano	7-8	5.17
8	1703/02/02/11:05	Aquilano	10	6.65
10	1461/11/26/21:30	Aquilano	10	6.46

Source <http://emidius.mi.ingv.it/DBMI11>

**Table 2** Historical seismicity at L'Aquila

Intensity at the L'Aquila city (MCS)	Year/month/day/hour	Epicentral area	Intensity at the epicentral site (MCS)	Magnitude moment (Mw)
9	1349/09/09	Aquilano	9	5.88 ± 0.31
9	1461/11/27/21:05	Aquilano	10	6.41 ± 0.34
9	1703/02/02/11:05	Aquilano	10	6.72 ± 0.17
8	1315/12/03	Castelli dell'Aquilano	8	5.57 ± 0.34
7-8	1791/01	L'Aquila	7-8	5.35 ± 0.34
7-8	1915/01/13/06:52	Avezzano	11	7.00 ± 0.09
7	1703/01/14/18:00	Appennino umbro-reatino	11	6.74 ± 0.11
7	1762/10/06/12:10	Aquilano	9	5.99 ± 0.34
7	1786/07/31	L'aquila	6	4.94 ± 0.36
7	1958/06/24/06:07	L'Aquila	7-8	5.21 ± 0.11
6-7	1750/02/01	L'aquila	6-7	4.93 ± 0.34
6-7	1805/07/26/21:00	Molise	10	6.62 ± 0.11
6-7	1916/04/22/04:33	Aquilano	6-7	5.10 ± 0.25

Source <http://emidius.mi.ingv.it/DBMI11>

**Fig. 6** The most affected areas surrounding L'Aquila city after historical seismic events by Baratta (1901)



seismic signals on soft and thick surficial sediments and where morphology and subsurface complex geometries are detected. Nonetheless, Table 2 shows 10 out of 13 seismic events that damaged L'Aquila with an Intensity degree higher than 7 and up to 9. Among others, the ones that damaged both L'Aquila and Onna cities caused higher degree of damages at Onna than at L'Aquilacity.



### 3 Main Features of the Surface Geology of the Aterno Valley

The Aterno Valley is a river tectonic depression hosting continental deposits since the Early Pleistocene. These deposits are constituted by mainly lacustrine, alluvial and colluvial sediments as well as landslide accumulations (Bosi and Bertini 1970). The Quaternary tectonic basin is elongated in the NW-SE direction and is bounded by predominately NW-SE-striking and SW-dipping active normal faults (Bagnaia et al. 1992) that generated elongated ridges in pre-Quaternary carbonate rocks and emerging from the continental deposits. As shown in Fig. 7, continental sediments were deposited inside the Valley, mainly belonging to lacustrine, fluvial and slope environments. The geological sequences observed within the Aterno Valley (Working Group MS-AQ 2010) consist of a sequence of units that can be detected only by drilling. Recently, a borehole at the L'Aquila downtown hill near the AQK seismic station has been performed up to 300 m. It showed a 250 m thick homogeneous sequence formed by clayey silts and sands laid upon carbonate bedrock (Amoroso et al. 2010). On the contrary, the Middle Pleistocene variably cemented calcareous breccias and dense calcareous gravels (the so-called L'Aquila Breccias) outcrop in several areas of the Aterno Valley and form the L'Aquila downtown hill. They are superimposed to the clayey-sandy-igniferous upper unit and the clayey-sandy unit. The L'Aquila Breccias are composed by clasts, whose size may reach even several cubic meters that came northward from the Gran Sasso chain. The Quaternary sequence continues with terraced fluvial deposits from the Aterno paleo-river (Vetio Stream unit) that are laterally in contact with alluvial-debris fan

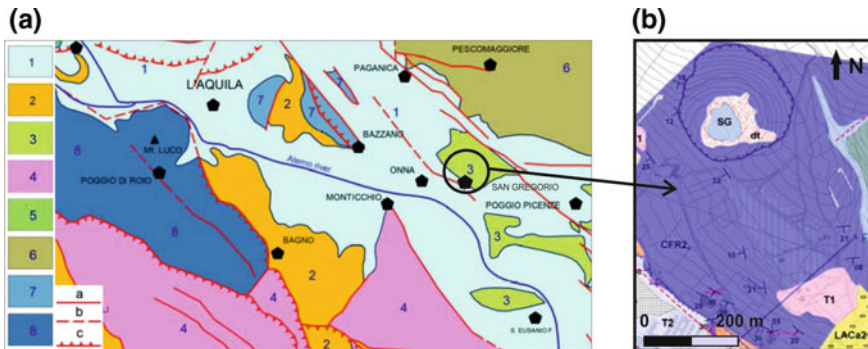


**Fig. 7** a Essential geological outlines of the Aterno Valley. 1 Continental deposits. 2 terrigenous units (upper Miocene). 3 Mesozoic platform and mioceniclimestones (area of Aterno River). 4 Cretaceous platform and mioceniclimestones (Ocre Mts.) and calcareous-marly-detrital lithologies. 5 Mt. Ruzza area. 6 Filetto-Pescomaggiore area. 7 Mt. Pettino area. 8 Hyp>Roio-Tornimparte area. a Normal fault. b Presumed normal fault. c Overthrust or transgressive fault. b Geologicalmap 1:5000 scale at San Gregorio site. SG: San Gregorio alluvial fan. T2: sandy silts and gravel. T1: gravel and conglomerate. LACa2: gravel. CFR2: calcarenite (After Working Group MS-AQ 2010 modified)

deposits (Mt. Pettino unit) corresponding to the sediment surface of Mt. Pettino. Finally, the youngest sediments exposed along the whole Aterno valley are dated to the Holocene-upper Pliocene age. Such deposits (unit 1, Fig. 7) are alluvial deposits consisting of alternations of more or less coarse gravels, sands and silty clays of fluvial and alluvial-fan environments organized in lenticular bodies associated with the catchment basin feeding the Aterno River. The lithological and geophysical characters of these recent continental deposits have been investigated in the framework of recent projects funded by the Italian Department of Civil Protection, over the last 5 years, as well as additional geotechnical and geophysical investigations for the microzonation studies performed in the most affected areas from the 2009 earthquake (Working Group MS-AQ 2010; Monaco et al. 2009 and Lanzo et al. 2011).

Figure 8 shows the location of five seismic stations installed in the Aterno Valley by the INGV before the 6th of April that recorded the main shock. Figures 9, and 10 display the shear wave velocity profiles derived from cross-hole and down-hole tests performed at those 5 seismic stations, that are: AQA, AQV and AQG in the upper Aterno valley and AQK at L'Aquila city center (Fig. 8). The results of lithological and seismic tests are available on the website [http://itaca.mi.ingv.it/ItacaNet/itaca10\\_links.htm](http://itaca.mi.ingv.it/ItacaNet/itaca10_links.htm). AQA (Fig. 9) and AQV (Fig. 10) stations are founded on Holocene deposits of alluvial origin, whose variable thickness is due to the deepening of the basin shaped carbonate bedrock. AQK station (Fig. 9a, b) is placed on the Aielli-Pescina Supersynthem, in particular the landslide carbonate breccias exposed at L'Aquila city center. Here, the breccias reach a depth of 40 m overlying stiff silts that show constant shear wave velocity value equal to 650 m/s up to the



**Fig. 8** Location of the seismic stations that recorded the main shock; (in red) locations of the epicenters of the main shock and some strong aftershock of 2009 L'Aquila earthquake

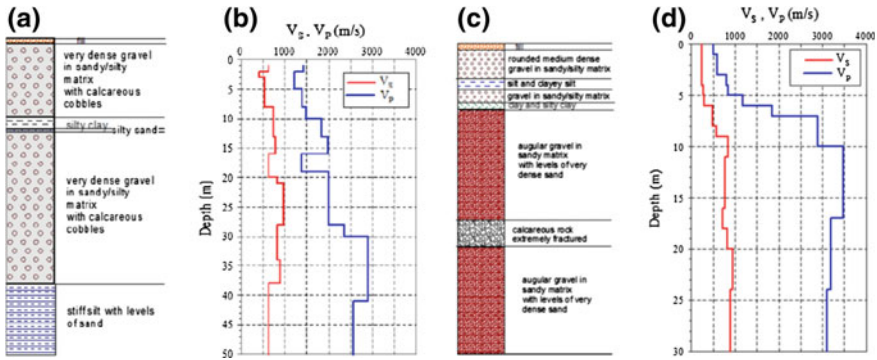


**Fig. 9** AQK seismic station characterization: **a** lithology; **b** seismic wave velocity profile. AQA seismic station characterization: **c** lithology; **d** seismic wave velocity profile

end of the sounding. This drilling doesn't intercept the bedrock that is the Mesozoic carbonate bedrock. Nonetheless, as mentioned before, a further deeper drilling has been recently performed near the AQQ station (Amoroso et al. 2010): it found this formation at a depth of 250 m.

At AQA (Fig. 9c, d) the breccias show typical rocky shear wave velocity value since a 9 m depth, that is 800 m/s. At AQV station, at the central sector of the valley (Fig. 10c, d), the carbonate bedrock is intercepted at a depth of 50 m.

Finally, the AQQ station (Fig. 10a, b) is placed on the edge of a valley to which AQV and AQA belong: AQV is placed at the center, AQA in the middle between AQV and AQQ. The lithological characteristics of the sequence under AQQ show fractured carbonate rock where shear wave velocity is 700 m/s as a mean value over the first 25 m thickness.

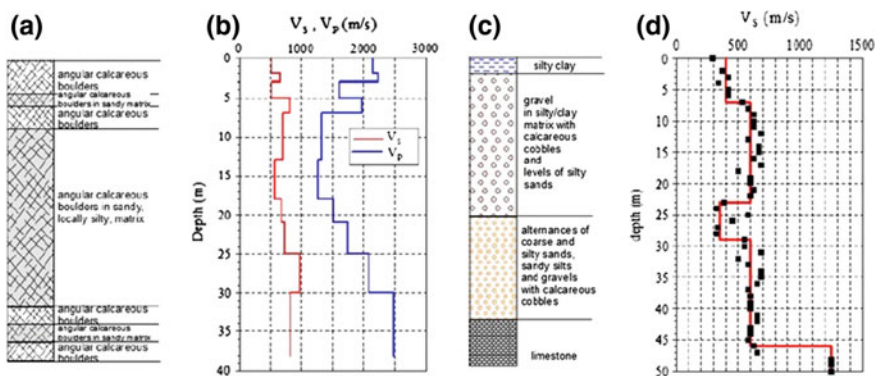


**Fig. 10** AQQ seismic station characterization: **a** lithology; **b** seismic wave velocity profile. AQV seismic station characterization: **c** lithology; **d** seismic wave velocity profile

Such lithological description by shear wave velocity profiles is useful, although preliminary, in local site response description. As the next section shows, the characteristics of the seismic records of the main shock at those stations cannot be fully understood if only “near field and source” effects are considered. On the contrary, when the local seismic behavior due to the complex surface geology is taken into account, the observed amplifications can be explained and even predicted by means of 1D numerical simulations, at a preliminary stage.

## 4 Seismic Monitoring Throughout the Southern Portion of the Aterno Valley

### 4.1 Seismic Monitoring at Urban Sites

Seismic monitoring has been carried out soon after the main shock of April 6th. Some weak aftershocks were registered at Onna, Monticchio and San Gregorio, as illustrated in Figs. 12, 13, 14 and at Villa Sant’Angelo and Tussillo (Figs. 15, 16, 17 and 18). An Array of four SSU Micro-Seismograph (GeoSonics Inc.) seismometers and two DAQLink III (Seismic Source Co.) seismometers with arrays of HS-1-LT 3C (Geo Space Corporation) geophones were used. The monitoring activity was undertaken by programming the velocimeters with a trigger threshold of 0.25 mm/s, a pre-trigger of 1 s, a sampling step of 0.003 s and a recording length of 15 s. The lower bound frequency that can be recorded by means of these velocimeters is 5 Hz, although 2 Hz is the lowest frequency that can be detected by these geophones according to their technical features (Fig. 11, Table 3). For the seismometers, the acquisition parameters were set as follows: sampling window of 0.004 s, recording duration of 80 s, the trigger threshold of 0.02 in./s and pre-trigger time duration of 10 s.

Few events recorded during the seismic monitoring were classified by the INGV office (with Magnitude and hypocenter depth), such as those in Figs. 12 and 13; however, all the records have been compared with the microzoning maps drawn by the Working Group MS-AQ (2010) that are hereafter (Figs. 16, 17, 18 and 19).

Figures 12, 13 and 14 relate to the three recorded events: on 21/04/2009 at 23:35 UTC with  $M_l = 2.6$  and hypocentre depth of 9.1 km (Fig. 12); on 21/04/2009 at 05:03 UTC with  $M_l = 2.5$  and hypocentre depth of 10.5 km (Fig. 13); on 22/04/2009 at 04:46 UTC with  $M_l = 2.6$  and hypocentre depth of 10.1 km (Fig. 14). Although the geophones were installed only 3 km away from each other, the peaks of the pseudo-velocity spectra (PPV) measured during these three seismic events show significant differences in the peak magnitudes and the amplified frequencies. In Fig. 12, sensor 4823, installed over the silty-clayey and sandy-gravelly alluvial deposits at Onna, measured the highest peaks in the area: from  $PPV = 1.27$  to 6.35 mm/s. At the same time, sensor 4824 installed at mid-slope on Monticchio calcareous rocks measured the lowest PPV values, varying from 0.46 to 0.56 mm/s.

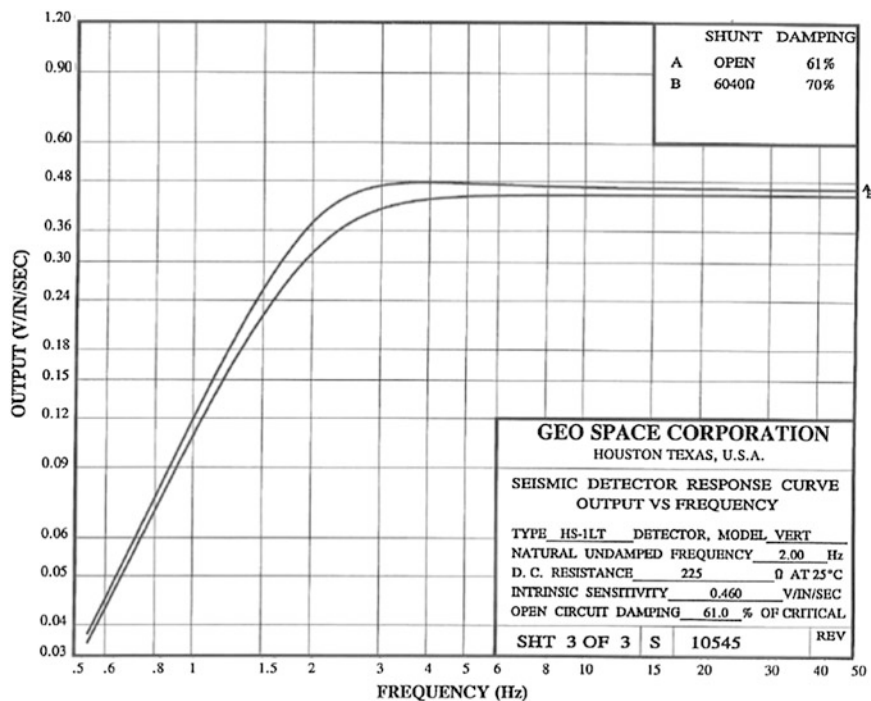


**Fig. 11** Technical features of HS-1-LT 3C (Geo Space Corporation) geophones

**Table 3** Technical features of SSU micro-seismograph (Geosonics Inc.)

Resolution	0.25 mm/s
Frequency range	2–250 Hz
Record length	15 s (1 s step)
Memory	Up to 20 events or (in continuous) 11 days
Accuracy	5 %

Furthermore, sensor 4826 installed at the top of the slope on calcareous rocks at San Gregorio measured a high PPV equal to 1.27 mm/s. An additional sensor (4825) was then installed over incoherent deposits at the entrance of a narrow valley, approximately 1 km far from Monticchio, South-westwards measured a PPV of 1.78 mm/s. Relating to the seismic event on 21/04/2009 at 23:35 UTC, the signal recorded at Onna shows a peak at a frequency of 7 Hz, whereas at Monticchio and San Gregorio the peak arises at 9-15 Hz. Similar responses are shown in Figs. 13 and 14 for the other two weak seismic events. Amplifications at low frequencies (lower than 2 Hz) at these sites could not be measured due to the instrumental limitations; however, the recorded velocity spectra are discussed here to quantify the local seismic effects. Thus, with respect to the earthquake event on 21 April 2009 at 23:35 UTC, the Onna PPV is 5 and 11 times higher than the San Gregorio



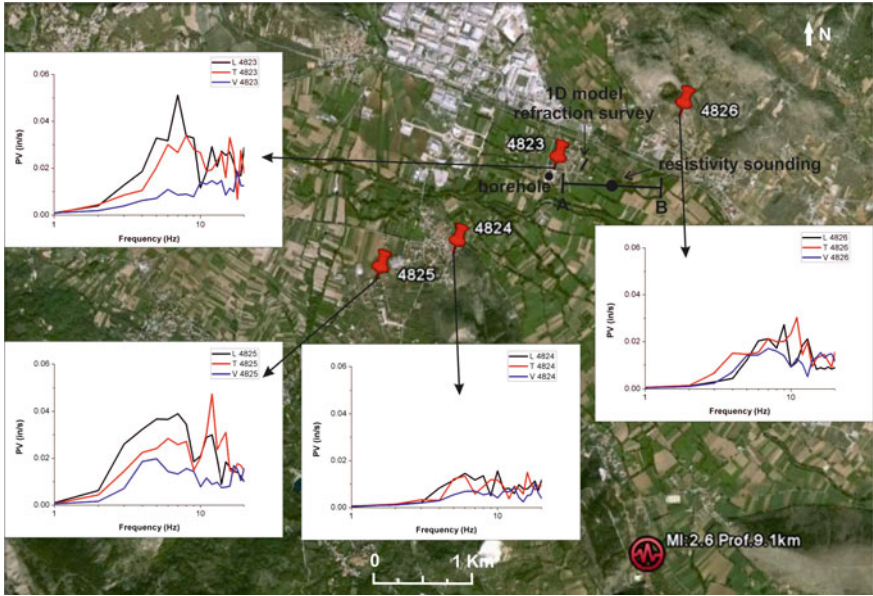


**Fig. 12** Earthquake event on 21 April 2009 at 23:35 UTC: Onna (4823) and Monticchio (4824 and 4825) monitoring site locations with velocity spectra (PV); geophysical surveys and borehole locations at the Onna site

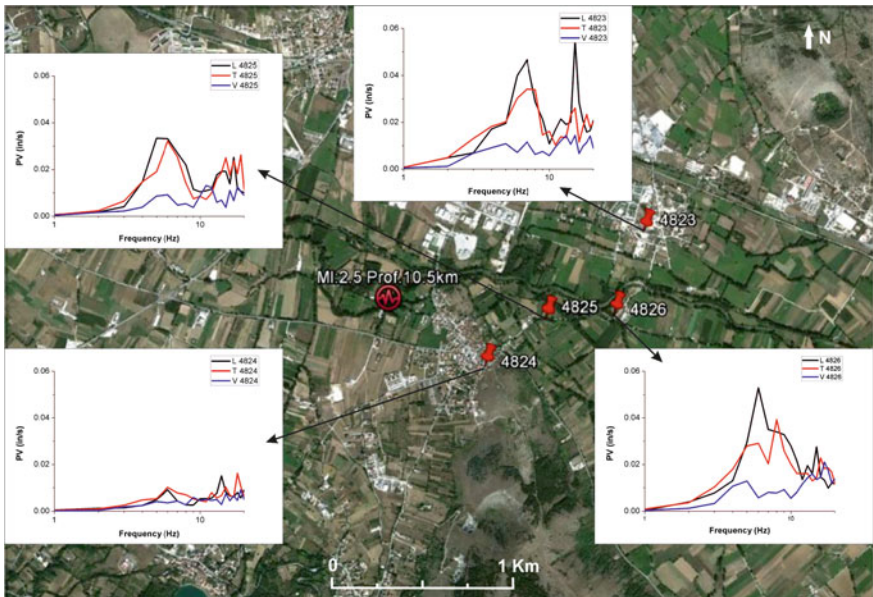


**Fig. 13** Earthquake event on 21 April 2009 at 05:03 UTC: Onna (4823), Monticchio (4824) and sites in between (4825 and 4826) monitoring sites locations with velocity spectra (PV); geophysical surveys and borehole locations at the Onna site

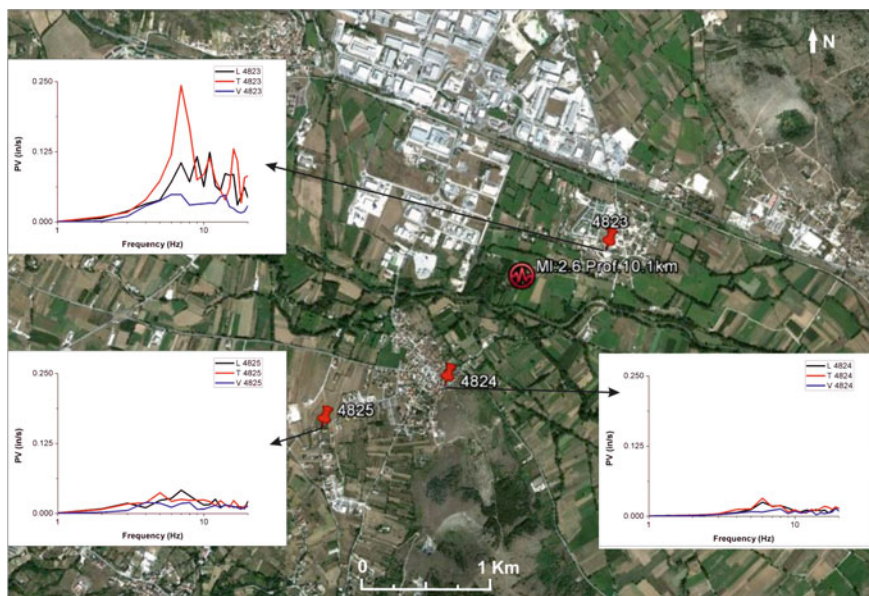


**Fig. 14** Earthquake event on 22 April 2009 at 04:46 UTC: Onna (4823) and Monticchio (4824 and 4825) monitoring site locations with velocity spectra (PV); geophysical surveys and borehole locations at the Onna site

and Monticchio ones. These differences in the measured spectra can be associated with different litho types, seismic impedance contrasts and possibly shear wave focalizations due to basin shape (Vessia et al. 2011) at Onna site and topographic relief at San Gregorio site. Moreover, the recorded PPV values reflect the differences in suffered damages. As a matter of fact, the difference in seismic responses among the three municipalities (Onna, Monticchio and San Gregorio) grows up to 3.5° on MCS intensity scale during the April 6th main shock event: Onna shows an  $I_{MCS} = 9.5$ , Monticchio an  $I_{MCS} = 6$  and San Gregorio an  $I_{MCS} = 9$  (Galli and Camassi 2009) (Fig. 5).

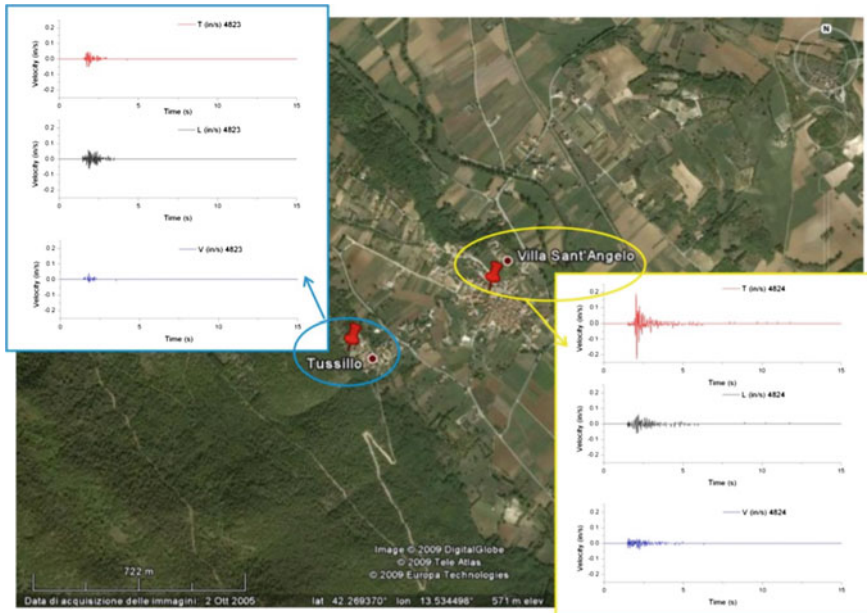
The microzoning map at Onna (Fig. 23b) has only been drawn. As a matter of fact, Monticchio was not involved in microzoning activities because of the low damages and seismic intensity. San Gregorio was investigated up to the first level of microzoning; however, 2D numerical analyses carried out in Sect. 5 (Fig. 31b) showed amplifications in the period range 0.35–0.45 s (2–3 Hz) (Fig. 36a).

The seismic monitoring has been developed also at Villa Sant'Angelo and Tussillo city centers by the same geophones used at Monticchio-Onna-San Gregorio site. These sensors were located in the historical center at Villa Sant'Angelo and on the outcropping rock at Tussillo. In these sites, the main shock of April 6, 2009 caused differentiated damages although the two centers are 800 m from each other: Villa Sant'Angelo suffered  $I_{MCS} = 9$ , whereas Tussillo suffered an  $I_{MCS} = 8$  (Galli and Camassi 2009). The sensors were installed during the period

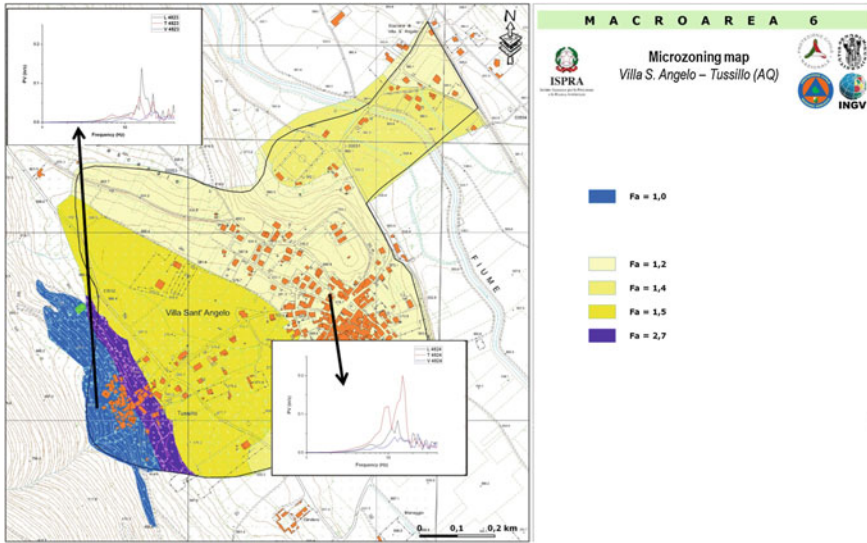
June 18–July 19, and on July 7, 2009 at 10:15 local time, a small event was recorded by sensors 4823 and 4824 (Fig. 15).

As can be seen in Fig. 15, comparing the three components recorded at Villa Sant’Angelo and Tussillo, it can be noted that the first site shows higher signal ordinates than Tussillo. The differences in the responses can be appreciated in Fig. 16, where the velocity response spectra are reported on the amplification map, drawn by the Working Group MS-AQ (2010). In this map,  $F_a$  is the Amplification factor calculated according to Eq. (1). Tussillo village is divided into two parts: one stable, that is  $F_a = 1$  and the other one that is amplified as  $F_a = 2.7$ . The event was recorded by the writers in the stable part. Looking at Fig. 16, the Villa Sant’Angelo site shows a higher amplification than the stable portion of Tussillo, although this latter amplifies the signal. The  $F_a$  at this point is 1. In particular, the peak of the velocity response spectrum is 0.23 in/s at Villa Sant’Angelo that is located over the sandy-gravelly and silty-sandy alluvial deposits whereas the peak at Tussillo is equal to 0.08 in/s on the outcropping rock. At both sites the peaks are about 15 Hz (0.07 s) although at Villa Sant’Angelo there is another peak in the velocity response spectra at about 10 Hz (0.1 s).

After this event, a stronger event on July 24, 2009 at 19:36 local time was recorded by means of two seismometers DAQLink III. They were located at the same points at Villa Sant’Angelo (historical center, in the municipal garden), whereas at Tussillo it was moved in the urbanized area (the one with a  $F_a = 2.7$  in



**Fig. 15** Seismic monitoring at Villa Sant’Angelo—Tussillo: the time history records relate to the small event occurred on July 7, 2009 at 10:15 local time



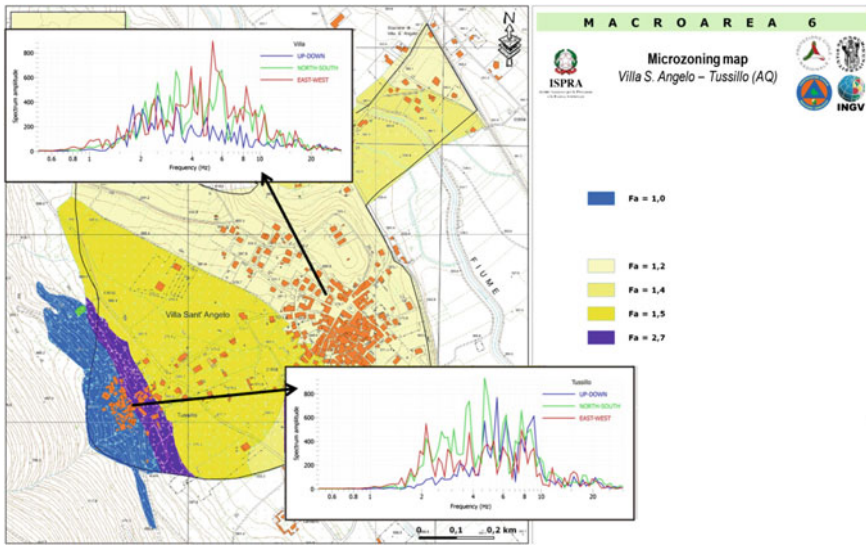
**Fig. 16** Velocity response spectra from July 7, 2009 at 10:15 local time records at both Villa Sant'Angelo and Tussillo compared with microzoning map drawn from Working Group (2010)

Fig. 17). Figure 17 shows the Fourier spectra of the three components at the two sites. In this second event, again, it is evident that points placed in amplified areas ranked  $Fa = 2.7$  or  $1.2$  show amplifications in the same ranges of frequencies and for the same amplitude. Maybe the use of the amplification factor cannot predict the differences either in amplified ranges of frequency nor in amplification amplitudes.

Similar evidences in recorded signals can be noted at the sites: Arischia (Macroarea 7, Fig. 18a, b) and Poggio di Roio (Macroarea 8, Fig. 19a, b). In the case of Arischia, three sensors DAQlink III have been set at three points in the urban area. As can be seen, from Fig. 18b, the three points are located on the three areas associated with three different amplification factors: the yellow one is  $Fa = 1.4$  and accordingly shows a lower amplification with respect to the other ones; the violet that is  $Fa = 2.7$  and the orange one that is  $Fa = 1.5$ . In spite of this classification, the velocimeters showed similar high amplifications, in terms of Fourier velocity spectrum over a range of periods  $0.01-0.14$  s ( $7-100$  Hz). This is actually in contrast with the classification based on  $Fa$ .

Finally, two velocimeters were located at Poggio di Roio city center less than 200 m from one another (Fig. 19a). All the urban area is classified as stable with  $Fa \leq 1$  (Fig. 19b). The records of the three components showed a different behavior of the two points: the first one does not amplify, the other one amplifies in the range of periods  $0.05-0.1$  s ( $10-20$  Hz). This is, again, in contrast with the classification based on  $Fa$  calculated values.





**Fig. 17** Velocity Fourier Spectrum of the event occurred on July 24, 2009 at 19:36 local time records at both Villa Sant'Angelo and Tussillo compared with microzonation map drawn from Working Group (2010)

## 4.2 Concluding Remarks on Seismic Monitoring

The seismic monitoring can be useful in microzonation studies for back-analysing the microzonation maps drawn through numerical methods. Amplification indexes, used for microzonation purposes, should be validated through the seismic monitoring with respect to (1) the amplified ranges of periods and (2) the amplification amplitudes compared site to site. From the monitoring activity performed at some sites within the Aterno Valley, the experimental evidences did not fit often with the seismic zonation expressed in terms of amplification factors  $F_a$ . Many reasons might be suggested: among others, (1) the inadequacy of the calculated amplification factor to interpret the filtering role of the surface geology on seismic records; (2) the need of validating 1D and 2D numerical simulations by means of weak and strong motion records at a site before using them to microzonation activities. Finally, the writing authors propose to use the *amplification functions* (both measured and calculated) to represent the “typical response” of a site, whether it is amplified or not.



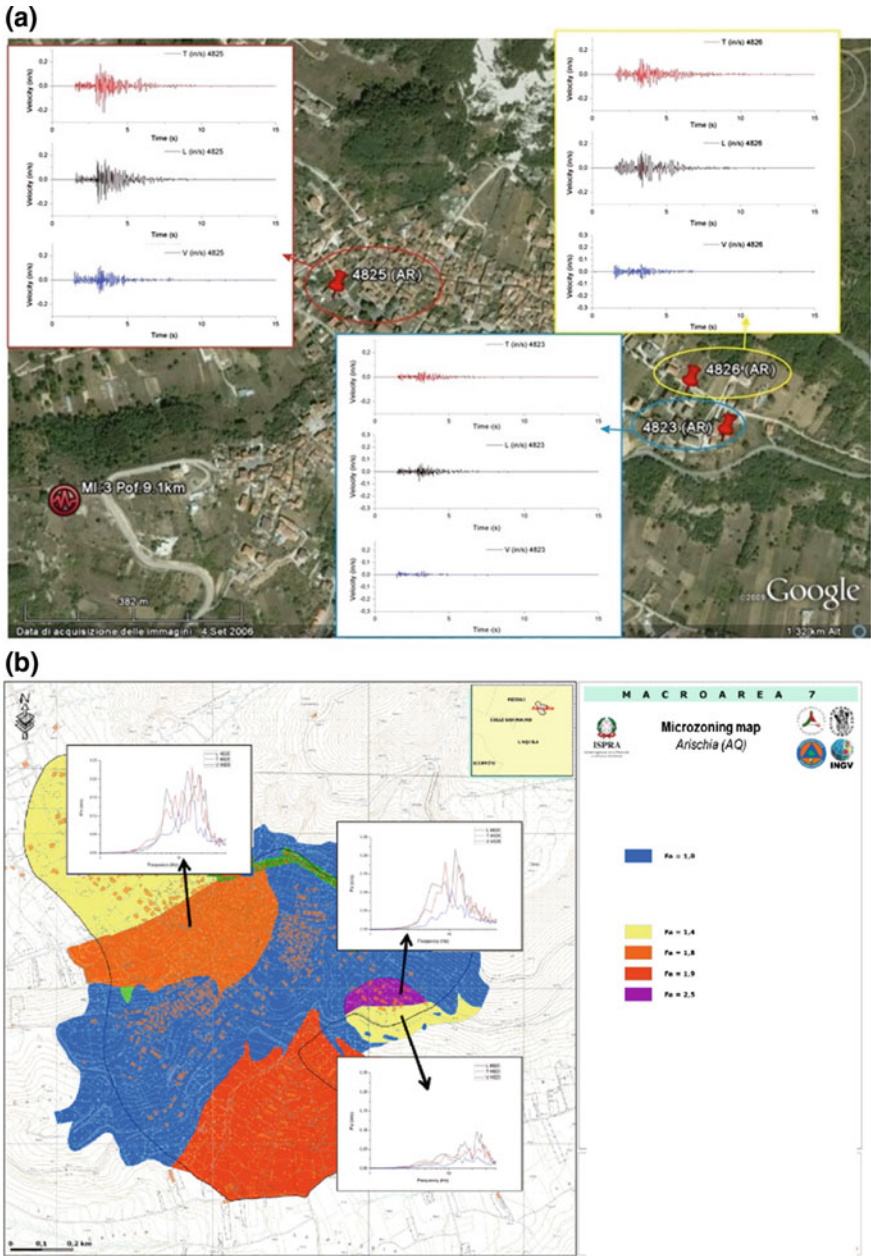
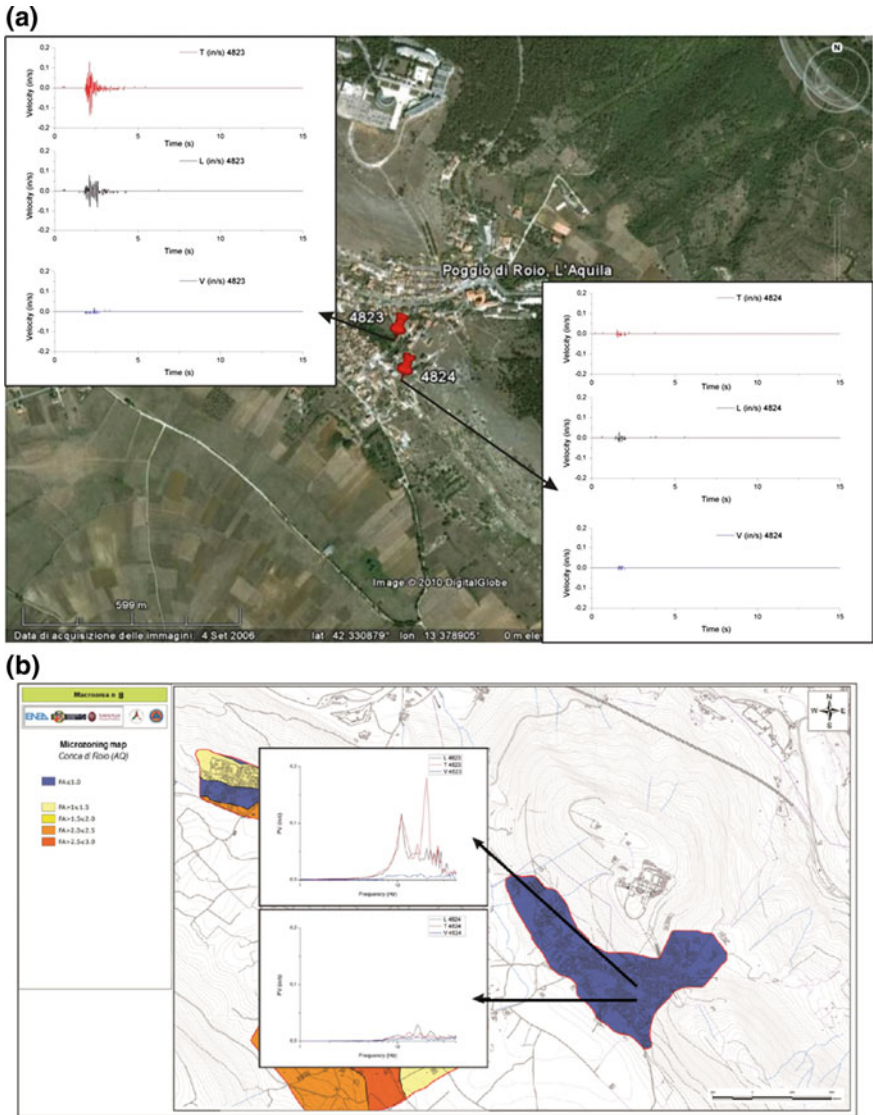


Fig. 18 Seismic monitoring at Arischia city center. Three velocimeters recorded the weak motion event on April 25, 2009 at 13:13 local time (MI 3; Prof. 9.1 km)



**Fig. 19** Seismic monitoring at Poggio di Roio city: two seismographs recorded the seismic event on April 18, 2009 at 20:40 local time. The two sensors were located at less than 200 m of distance

## 5 Numerical Simulations of Seismic Amplification Within the Aterno Valley

### 5.1 Some Evidences from the Main Shock Records

Five seismic stations recorded the main shock event on April 6, 2009 at 1:32 UTC within the Aterno Valley: they are shown in Fig. 8. Three out of five (AQA, AQQ and AQV) stations are placed in the northern part of the Aterno Valley, along a basin shaped seismic bedrock, whereas the others (AQU and AQK) are placed at L'Aquila city center. The two groups of seismic stations show similar distances from the epicenter, as shown in Fig. 8 (varying between 4.4 and 6.0 km), although the first group (AQA, AQV and AQQ) is placed more than 10 km far from Paganica fault. Four out of five stations have been seismically characterized by means of wave velocity profiles (Figs. 9 and 10): only AQU station, placed in the castle of L'Aquila city, is not characterized. Nonetheless, in the present study the acceleration spectrum registered at AQU has been plotted with the others in Fig. 20: the color identifies the station, the line type the component: solid line for UP component, dotted line for NS and broken line for WE components.

Despite the distance from the fault, Fig. 20a, b show that:

1. with respect to the vertical component, the maximum peak in the acceleration spectra is shown at AQV, then at AQA, AQK and AQU. These three sites show Holocene sediments with decreasing thickness. This is true also for the horizontal components, as can be easily noticed from Table 4;
2. the vertical peaks are all aligned on 19–20 Hz except for AQQ (Table 5). If “near field” or “directivity” effects are relevant, the responses at AQQ, AQV and AQA will be quite the same. On the contrary, the lowest peak and the lowest frequency is shown at the seismic station where fractured rock outcrops;
3. the horizontal peaks seem to occur at lower frequencies than the vertical ones: it could be due to the seismic properties of the lithological sequences of soil layers and geometric effects. Accordingly, from Table 5, along the valley that is oriented SW-NE, the AQQ, AQA and AQV stations show their peaks at different frequencies. Moreover, the peaks are comparable between AQA and AQV, whereas at AQQ, they are far lower. Such behavior recalls the basin effect (among others Vessia et al. 2011; Vessia and Russo 2013; Rainone et al. 2013).
4. from the inspection of Fig. 20a, b it can be noticed that the vertical components amplify shorter ranges of periods 0.04–0.2 s (2–25 Hz) with respect to the horizontal ones 0.08–0.6 s (1.7–12.5 Hz). On average, the peaks of the acceleration response spectra in vertical and horizontal components are similar.

As already mentioned, all the stations but AQU, have been characterized by means of a sounding and a Down Hole test published on the website: [http://itaca.mi.ingv.it/ItacaNet/itaca10\\_links.htm](http://itaca.mi.ingv.it/ItacaNet/itaca10_links.htm). Here, the main features of this characterization have been summarized in Table 6. The seismic bedrock has not been detected under all the stations, although at different depths as well as for different shear wave

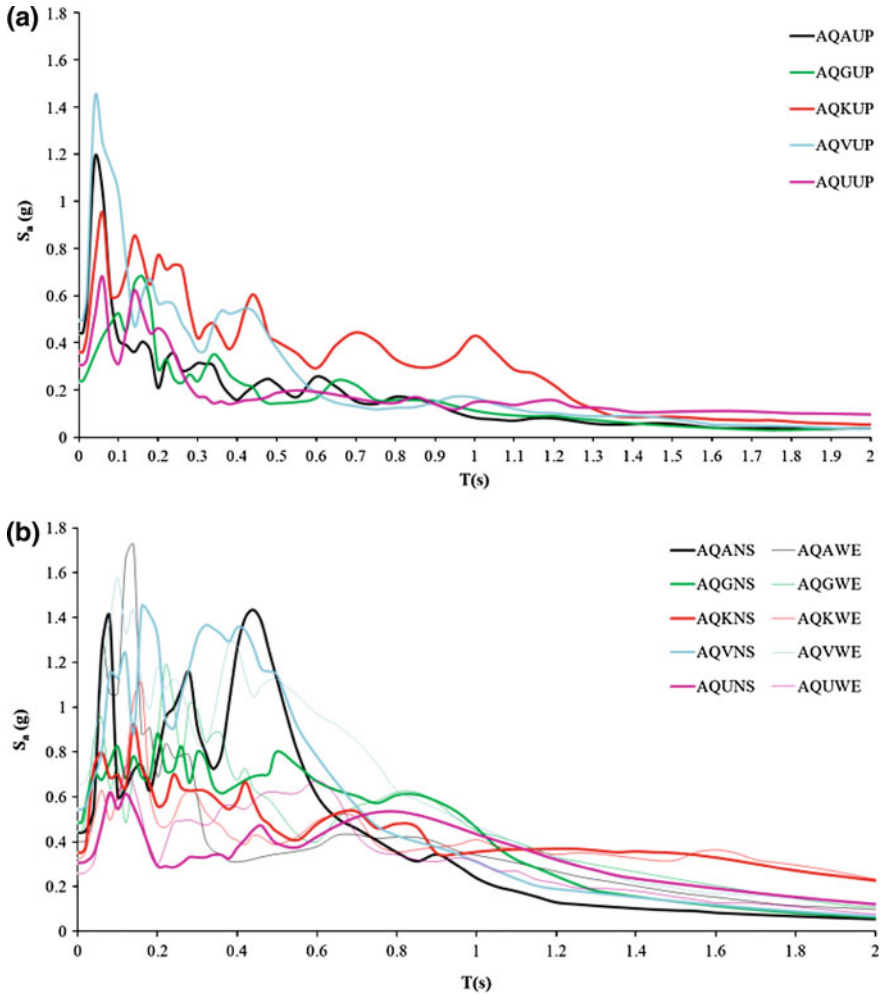


**Fig. 20** Acceleration spectra of the three components of the main shock registrations at the five seismic stations considered: **a** Vertical component (UP); **b** Horizontal components (NS-WE)

**Table 4** Peak of the acceleration spectra (g) for each main shock component at seismic stations within the Aterno Valley

Station code	WE	NS	UP
AQK	1.1	0.94	0.99
AQA	1.74	1.65	1.55
AQV	1.79	1.52	2.36
AQG	1.20	0.89	0.79
AQU	0.85	0.70	1.29

**Table 5** Amplified frequencies (Hz) in the acceleration spectra related to the three components of the main shock at five seismic stations

Station code	WE	NS	UP
AQK	6.2	25	20.8
AQA	7.2	17.8	18.9
AQV	9.0	5.4	20.8
AQG	4.5	5.0	6.6
AQU	7.8	7.6	19.6

**Table 6** Seismic properties of the soil under the seismic stations that recorded the main shock

Seismic station	$V_{S30}$ (m/s)	Bedrock depth (m)	Mean $V_S$ over the bedrock depth (m/s)	Shear velocity contrast $C_V$
AQK	717	13	622	1.25
AQA	552	9	342	2.36
AQV	474	47	523	2.42
AQG	685	25	651	1.5
AQU	–	–		–

velocity seismic profiles,  $V_S$  mean values have been calculated. Moreover, the shear velocity contrasts have been calculated (that is the ratio between the shear wave velocities of the bedrock and the overlying sediments) and reported in Table 6.

Considering the weighted mean value for shear wave velocity over the bedrock depth (fourth column in Table 6), it can be seen that AQV and AQA show the first and the second highest velocity contrasts  $C_V$  respectively. Such parameter plays a relevant role in surficial amplifications.

Comparing Tables 4 and 6 it can be noted that the highest horizontal peaks are registered at those stations that are far away from the Paganica Fault but are characterized by higher velocity contrast with respect to AQK and AQU, placed at L'Aquila city center (nearer to the Paganica fault). AQK shows a first seismic bedrock at 20 m, made up of L'Aquila "megabrecce" formation, that is very dense gravel in sandy matrix with calcareous cobbles: the mean value of shear wave velocity  $V_S$  within the first 20 m depth is 900 m/s. The megabrecce overlies the stiff silts that probably reach a 250 m depth and shows  $V_S = 622$  m/s as a mean value over the bedrock (Table 6).

Comparing the peaks at AQK and AQG in a W-E direction, it can be noted that the second station is more amplified, although the shear wave mean value over the bedrock is similar (Table 6). On the contrary, the velocity contrast at AQG is higher than at AQK. The seismic bedrock at AQG is 25 m deep, whereas at AQK there are two seismic bedrocks: one at 20 m and the other at about 250 m. From the response characters highlighted, the role of surface geology seems to be significant although difficult to identify and quantify. For instance, the highly amplified frequencies can be related to the high frequency content of the seismic signals in "near-field" conditions, but further studies are needed for shedding lights on the influence of the



local seismic response of heterogeneous surface geological conditions at high frequency contents. However, the amplified high frequencies seem to be also affected by seismic properties of soils and structures or buildings, that can be estimated by measuring the resonance frequencies of both soil and structures (Rainone et al. 2010; Vessia et al. 2012). Finally, further evidences from the Lanzo et al. (2010) study highlighted the relevance of local amplifications in the 2009 L'Aquila earthquake. Accordingly, Fig. 21 shows 5 % damped pseudo-acceleration response spectra for four stations on the hanging wall of the fault. Such spectra are related to the motions rotated into fault normal and fault parallel directions, based on the  $147^\circ$  strike reported in the Earthquake setting and source characteristic section. According to Lanzo et al. (2010), the plot shows:

1. no evidences of significant polarization of ground motion in the fault normal direction, that is related to the rupture directivity;
2. a significant energy content at high frequencies, 10–20 Hz. Focusing on the period range 0.3–1.0 s, the spectral ordinates at AQA and AQV stations, overlying soft sediments, are larger and relatively more energetic than AQQ and AQK stations, founded on firmer soils.

This study strengthens the role played by local and surface geology on amplification phenomena in near field conditions. Some 1D simulations have been performed at Onna site and L'Aquila city center, at the seismic station called MI03 and AQK. Unfortunately, MI03 didn't register the main shock. The present numerical simulations have two main objectives: (1) to stress the influence of the litho-technical description of surficial geological sequences for predicting amplification phenomena and (2) to suggest an operating approach for characterizing the amplification at the site in microzoning studies.

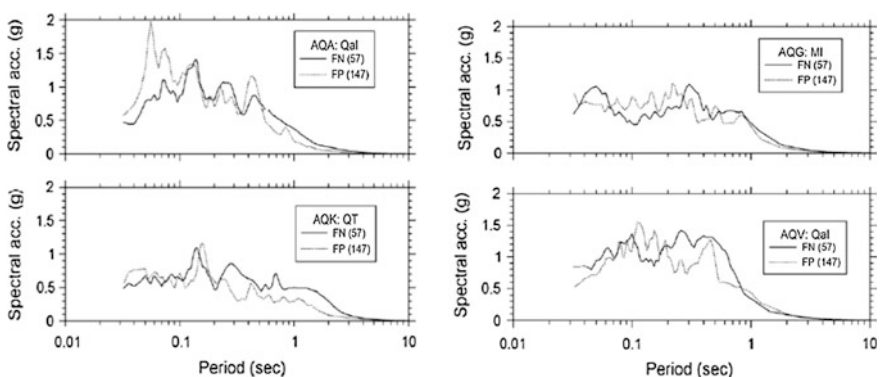


**Fig. 21** Acceleration spectra from main shock records on the hanging wall of the Paganica fault (after Lanzo et al. 2010)

## 5.2 *Predicting Local Seismic Response at Onna (Macroarea 5) and L'Aquila City Centers (Macroarea 1) by Means of Numerical Simulations*

### 5.2.1 One-Dimensional Analyses

One-dimensional (1D) numerical simulations have been performed to overpass some inconsistencies between the strong-motion records and the proposed strategies for local seismic response prediction at L'Aquila city center, identified as Macroarea 1 (Fig. 2).

The first seismological studies pointed out: (1) the impulsive character of the recorded signals, (2) their high frequency content, (3) the south-eastern direction of the peak ground accelerations and increasing velocities according to the directivity effects of the rupture propagation along the Paganica fault, (4) the recorded vertical components higher than the horizontal ones according to near-field conditions. Despite the common agreement on the abovementioned phenomena, some relevant exceptions have been observed at some seismic stations: AQV registered anomalous highly amplified horizontal components with respect to AQK or AQU. Moreover, some anomalous heterogeneous damages occurred at neighboring sites, suggested to investigate the role of local geo-lithological conditions on the heterogeneous damaging. For instance, the main shock provoked severe damages and many fatalities throughout Onna city (MCS = IX – X), whereas at the Monticchio site, that is less than 2 km far from Onna, a few damages caused a MCS VI seismic intensity. Figure 12 shows the great differences in amplifications registered for a minor aftershock (Mw 2.6 and hypocenter depth at 9.1 km) that occurred on April 21, 2009 at 23:35 UTC, at the two sites. Thus, for those areas where the MCS intensity was higher than VI, microzonation maps have been drawn (Working group MS-AQ 2010).

At level three, microzoning maps are derived from the calculated amplification factor  $F_a$ . The  $F_a$  is defined according to the following procedure (Gruppo di Lavoro 2008).

1. To identify the period corresponding to the maximum ordinate  $P_M$  of the Input ( $TA_i$ ) and the Output ( $TA_o$ ) acceleration spectra.
2. Centered on  $P_M$ , the following mean values of input ( $SA_{m,i}$ ) and output ( $SA_{m,o}$ ) acceleration spectra are calculated (Gruppo di Lavoro 2008):

$$F_a = \frac{SA_{output}}{SA_{input}} = \frac{\frac{1}{T_a} \int_{0.5P_M}^{1.5P_M} SA_{output}(T) dT}{\frac{1}{T_a} \int_{0.5P_M}^{1.5P_M} SA_{input}(T) dT} \quad (5.1)$$

where  $SA(T)$  is the acceleration spectrum: the output is related to the results of 1D and 2D numerical simulations, and the input is the strong motion signal used as input motion in the same simulations.  $T_a$  is the amplified period within the

acceleration spectra. Although quantitative micro-zoning procedures have been carefully defined and explained, many critical points arise from the microzoning maps reported in Fig. 22. Figure 22a shows the undefined Fa value within the blue area where the AQK station is placed. At the same time, Onna city is classified as  $Fa = 1.8$  with a complete destruction of small buildings whereas some portions of L'Aquila city are ranked  $Fa = 1.9$  or  $2.0$  with no correspondence with damages.

Thus, the authors try to suggest a simple method for relating the litho-technical properties of a sequence of surface sediments to the amplified seismic response. To this end, 1D simulations have been carried out on a few possible sedimentary sequences at AQK and MI03. The code used is EERA (Bardet et al. 2000) that simulates the non-linear seismic response of soils by means of the equivalent linear constitutive law. This seismic behavior model needs shear modulus reduction curve  $G(\gamma)/G_{\max}$  and damping increasing curve  $D(\gamma)$  measured by laboratory tests for each litho type, e.g. resonant column, cyclic triaxial equipment. For the present simulations, the curves measured by Working Group MS-AQ (2010) for investigated soils at macroareas 1 and 5 have been used. Moreover, the input motions considered are the ones illustrated in Fig. 23, provided by Pace et al. (2011) for microzonation studies carried out in the mentioned macroareas:

1. the uniform hazard spectrum of the Italian Building code (NTC08). It is a lower bound spectrum of 2009 L'Aquila earthquake;
2. a probabilistic uniform hazard spectrum with a return period of 475 years.; it has been obtained by two source models named LADE1 and SP96 GMPE (Pace et al. 2011). This spectrum gives an upper bound spectrum to L'Aquila earthquake, reaching a maximum spectral value of about 1 g at 0.25 s;
3. a deterministic spectrum obtained from SP96 GMPE for a magnitude-distance pair ( $M_w$  6.7,  $Repi = 10$  km). The deterministic spectrum gives intermediate spectral values ranging from 0.35 g at 0 s, to 0.8 g at 0.25 s and 0.4 g at 1 s.

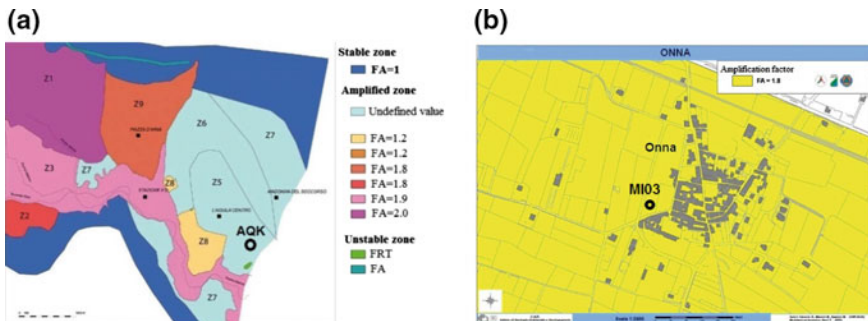


**Fig. 22** a Macroarea 1: seismic microzonation of level three at L'Aquila center (after Working Group MS-AQ 2010 modified); b Macroarea 5: seismic micro-zonation of level three at Onna city

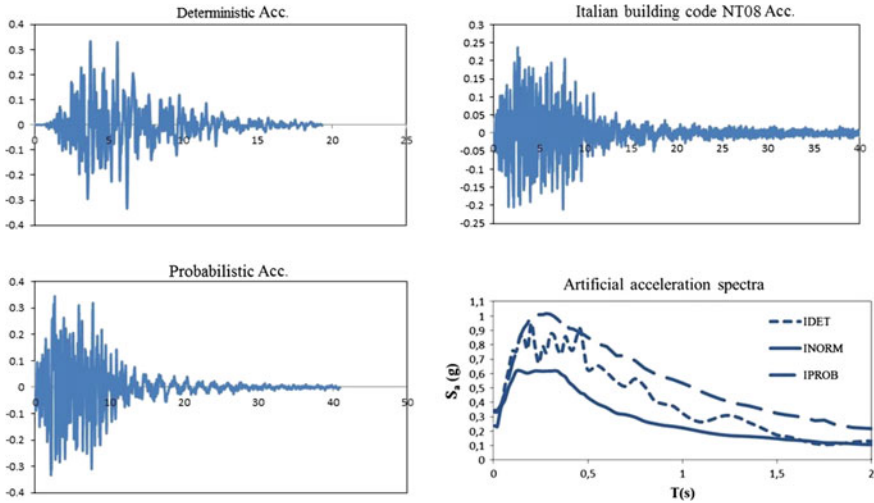


**Fig. 23** Artificial input motions simulating 6th April 2009 main shock used for numerical analyses within Macroareas 1 and 5

The 1D numerical study presented here considered two models for the sediment sequence under the AQK station (Fig. 24a) and two other models under the MI03 station (Fig. 24b). The two models at AQK concern different points of view about

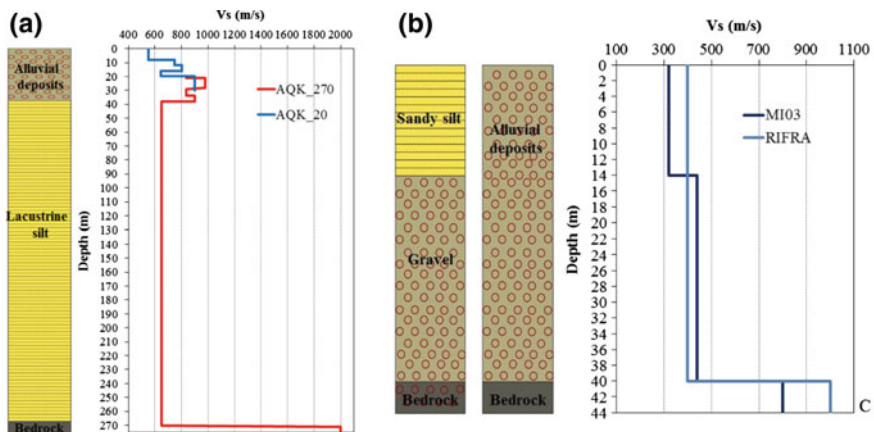


**Fig. 24 a** SH wave velocity profiles under AQK station for 1D numerical analyses. On the *left*: lithological model; on the *right*, two velocity profiles: Model 1 (in *blue*), bedrock at 20 m depth; Model 2 (in *red*), bedrock at 270 m depth. **b** SH wave velocity profiles under MI03 station for 1D numerical analyses. On the *left*, two lithological models; on the *right* the corresponding velocity profiles: Model 1 (in *black*): sandy silt up to 14 m and gravels up to the bedrock at 40 m depth. Model 2 (in *blue*): lithological succession of sand, silt and gravels called “alluvial deposits” up to the bedrock at a 40 m depth

the role of the velocity contrasts within the Holocene sequences, here named “alluvial deposits”. As mentioned before, the heterogeneity of the most recent and surficial sediments result in wave velocity inversions within the first 20 m depth. Such fast strata, according to the present authors, can be considered as preferential paths for seismic waves, playing the role of “hanging bedrocks”. This idea is an alternative to the common standpoint that poses the seismic bedrock approximately at about 250 m depth that is the geological bedrock. Here, at AQK, such a bedrock has been found at 270 m (Amoroso et al. 2010). Similarly, under the MIO3 station at Onna city center (Fig. 24b), the seismic bedrock has been reached at 40 m without any velocity inversions. The sedimentary sequence published by Working Group MS-AQ (2010) shows a downwards-graded increase in shear wave velocity values. The authors performed a refraction test, in 2009, from which the sequences of sands and gravels show a mean value of 400 m/s up to the bedrock depth where a 1000 m/s has been found: the bedrock shear wave velocity value is higher than the one suggested by the Working group MS-AQ (2010). Thus, the second model suggested by the writing authors put in evidence the presence of a velocity contrast  $C_v = 2.5$  instead of 1.8. Such condition, from the author standpoint, can influence the local response of the sediments by increasing surficial amplification. The results of the abovementioned 1D numerical analyses concerning AQK are presented in Fig. 25a, b and Fig. 26a, b and concerning MIO3 in Fig. 27. Figure 25a shows, in blue, the output acceleration spectra calculated for the 20 m-bedrock model, whereas in black, the input acceleration spectra deconvolved at the depth of the seismic bedrock. In the same plot the acceleration spectra of the main shock horizontal components recorded at the AQK station have been reported. Model 1 amplifies the same periods keeping the shape of the input acceleration spectra; thus, such model does not change the input frequency content. Looking at Fig. 25b, from the shape of the amplification function  $A_f$  can be seen that the model amplifies the period range 0.05–0.2 s (5–20 Hz) that is the amplified range of periods in the NS and WE components of the main shock at AQK station.

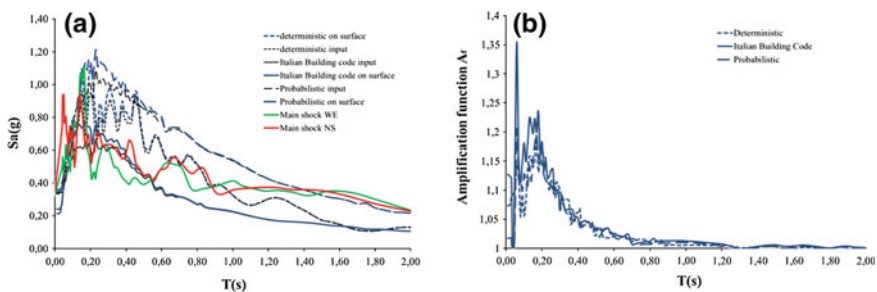


**Fig. 25** 1D numerical analyses results at AQK, for Model 1: **a** Acceleration spectra; **b** Amplification function  $A_f$



Hence, the Model-1 response is influenced by the input motion, but it amplifies those high frequencies as shown in the strong motion registrations. The amplification extent varies from 1.2 to 1.35; thus, according to Model 1, the AQQ site is strongly influenced by the input frequency content that is moderately amplified. Figure 26a shows the output acceleration spectra of Model 2, where the seismic bedrock is set at a 270 m depth. In this case, the frequency content of the output spectra is changed and the amplified periods are the longer ones. As can be better understood by Fig. 26b, the recorded strong motion NS and WE components show amplified periods lower than the ones amplified by Model 2. As a matter of fact, the periods amplified are higher than 0.20 s. This is true for the three inputs. Finally, although the site response is conditioned by the input motion, the two analyzed models show how relevant can be the contribution of the litho-technical model in modifying the amplified ranges of periods/frequencies. In the case of AQQ, the model of the “hanging seismic bedrock” fits better than the model with the “geological bedrock” to the measured records at the AQQ site (Fig. 26).

For the case of the MI03 station at Onna city, Fig. 27a shows the site responses of two models: one suggested in this paper (RIFRA, in blue) and the other accepted by Working Group MS-AQ (2010) (MI03, in red). The three input motions have been deconvolved at 40 m: both models show higher amplifications with respect to the AQQ station but Model RIFRA amplifies a broader range of periods, from 0.2 to 0.7 s. It is true for the three inputs and the amount of this amplification can be read in Fig. 27b: up to 1.5 at 0.2 s (5 Hz) and up to 2.4 at 0.5–0.7 s (2–1.43 Hz). The other model (MI03) produces lower amplifications (up to 2) in a narrower period range (0.2–0.55 s). Unfortunately, at MI03 no main shock records are available. Nonetheless, Di Giulio et al. (2011) analyzed three strong aftershocks registered at MI03 that occurred on 9th April with MI 5.4, 5.1 and 5. They show a large spectral content in horizontal components for  $T < 0.3$  s, and a spectral peak at 0.4 s with relative amplification level of 5, on average. Moreover, the shapes of spectral ratios between MI03 registrations and a reference bedrock site indicate amplifications in a large frequency band, up to 10 Hz (0.1 s). At MI03, the resonance frequency derived from the spectral ratio between the recorded horizontal and vertical components, for the case of the MI 5.4 aftershock, shows a spectral peak at 1.8 Hz (0.6 s). Thus, in the case of the MI03 seismic station, the Model RIFRA proposed by the writing authors better explains the main characters of the strong motion registrations. Accordingly, the role of the velocity contrasts seems to be relevant at both sites. Finally, in order to suggest a practical method for measuring the possible amplifications at the site, the amplification function  $A_f$  can be employed joined to the litho-technical models that correctly interpret, according to 1D simulations, the role of the velocity contrasts and the velocity inversions in the sediment sequences. Moreover, the AQQ model here proposed can be used at the L'Aquila site where deep geological bedrock is associated with surficial velocity inversion. Finally, an accurate seismic characterization of the surface sediment behavior is needed for reproducing the relevant features of the local seismic response. As can be seen, at MI03, two-dimensional numerical simulations are needed.

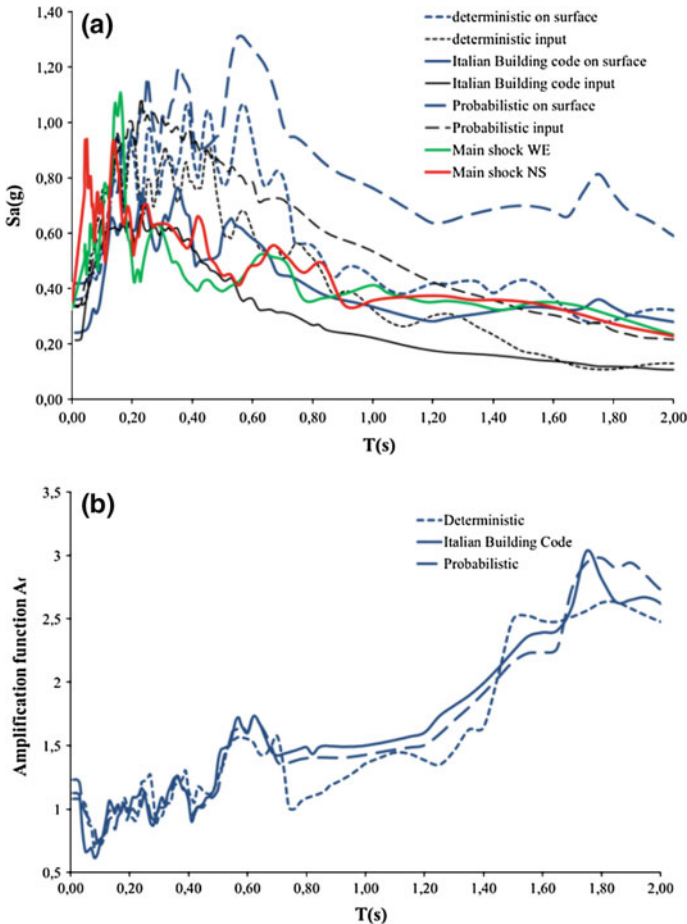


**Fig. 26** 1D numerical analyses results at AQK, for Model 2: **a** Acceleration spectra; **b** Amplification function  $A_f$

**5.2.2 Two-Dimensional Analyses at Macroarea  
5—Onna-Monticchio-SanGregorio Alignment**

A geological cross section of the Monticchio-Onna-San Gregorio alignment is shown in Fig. 28, suggested by Working group MS-AQ (2010). In the central portion of this cross section, where the mean elevation is 580 m, the following lithological sequence can be sketched from the surface to the basement: a very thin layer of Holocene deposit (unit 3), calcareous alluvial and fluvial deposits of sand and gravel with interbedded clay and silt, overlying Pleistocene silty-clay sediments (unit 2); approximately a 50 m depth of lower Pleistocene conglomerate substrate (unit 1). The deep basement is assumed to be the Mesozoic limestone/Flysch that

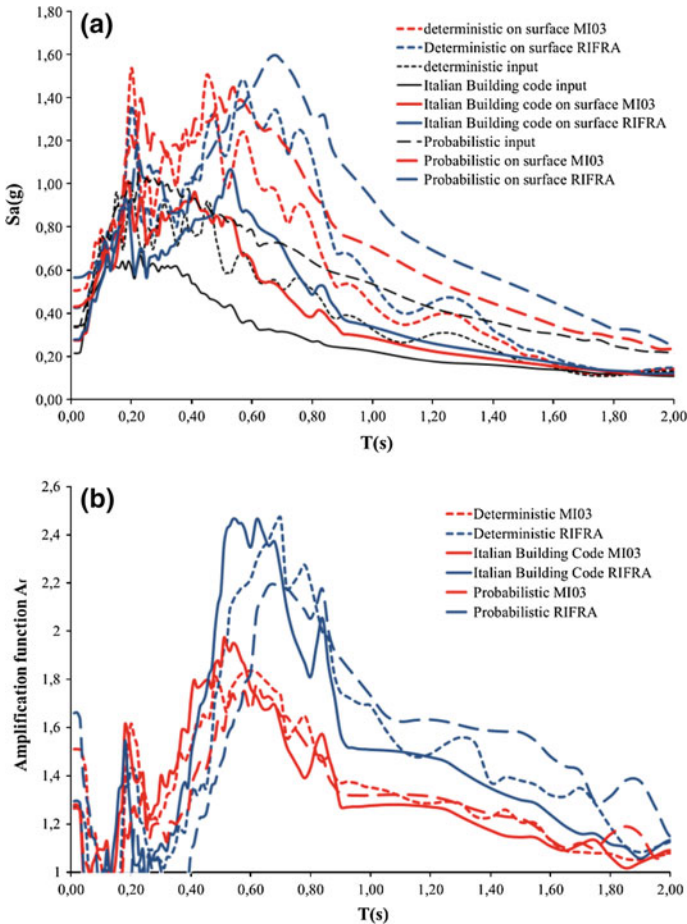


**Fig. 27** 1D numerical analyses results at MI03, for Model 1 (in red) and Model 2 (in blue): **a** Acceleration spectra; **b** Amplification function  $A_f$

outcrops in the uppermost Monticchio village (Di Giulio et al. 2011). This village is built on a gentle slope at the toe of the northern part of the Cavalletto Mountain at an approximately 600 m elevation.

Monaco et al. (2009) recently drilled a boring on the western plain of Monticchio for geotechnical characterization (Fig. 29c, borehole in red nearby Monticchio). Calcareous gravel and cobbles were found down to the bottom of the borehole, at 40 m (Fig. 29a). The eldest continental deposits (early Pleistocene) consist of very stiff or cemented lacustrine carbonate silt with inter-bedded sand that crop out at San Gregorio (APAT 2005). The geological relieves and two- electrical resistivity tomography (ERT) carried out at San Gregorio, show the well-stratified

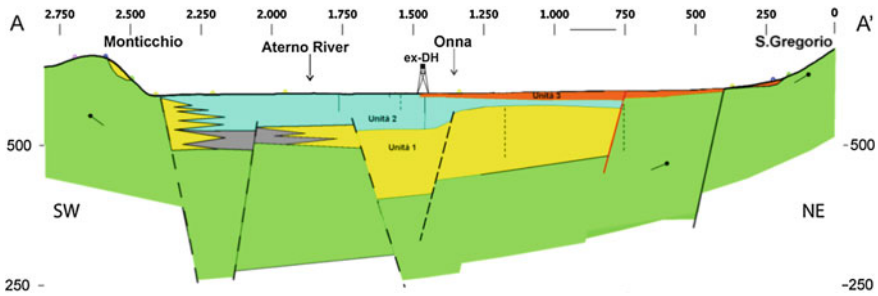


**Fig. 28** Geological setting along a section crossing the middle Aterno Valley (After Working group MS-AQ 2010 modified). *Unit 1* conglomerates and gravel. *Unit 2* alternation of gravel, sand and silt. *Unit 3* eluvium-colluvium made up of soft silt and clay with scattered gravel grains. *Green unit* limestone or flysch bedrock. The cross section vertical scale is magnified by 2

bio-clastic calcarenite bedrock outcropping on the western flank of the San Gregorio hillside (named “calcareniti a foraminiferi”, CFR2 in Fig. 7b).

This unit is locally intensely fissured. Geological and geophysical investigations were performed at Onna (Macroarea 5) for microzoning studies. Figure 29b shows some of the numerous field tests performed by Working group MS-AQ: one seismic refraction line (L7-SRZ1), two down-holes, soundings at 30 m depth, sounding at 60 m depth, micro-tremor measures (Nakamura technique), three geo-electric lines (ERT), among others. Accordingly, at Onna the quaternary continental deposits are made up of eluvium-colluvium of a few-meter thickness overlaying fluvial and alluvial units, more than 60 m deep. The geological bedrock was not intercepted by the soundings although a seismic bedrock was found by means of the refraction line, characterized by a shear wave velocity equal to 1000 m/s (Rainone et al. 2010). It is reported in Fig. 29c (refraction survey in black).

The refraction seismic surveys in P and SH waves, were processed by tomographic techniques (Fig. 30a). Furthermore, a resistivity depth sounding was carried out to identify the depth of the geological bedrock. The results of the two geophysical surveys are reported in Fig. 30a, b. They show that alluvial deposits can be detected up to a 100 m depth, under the first 2 m of cover. The deposits are characterized by two electrical horizons that are 63  $\Omega$  m resistivity as deep as 45 m and 48  $\Omega$  m up to 106 m. Furthermore, a high resistivity unit of 240  $\Omega$  m has been detected downwards. It is assumed as the geological bedrock. Nonetheless, the refraction line shows the seismic bedrock at about 40 m with a shear wave velocity equal to 1000 m/s (Fig. 30a). Moreover, the writing authors performed a borehole up to a 60 m depth near the MIO3 station (Fig. 29d). The stratigraphy shows, according to the velocity profile “RIFRA” (Fig. 30c) a new lithological horizon at about 40 m characterized by small carbonate clasts called “gravel” and sand in Fig. 29d. This 5 m stratum overlays stiff silty sand and sandy silt that show higher  $V_S$  values higher than 800 m/s up to 50 m. These  $V_S$  varies between 750 and

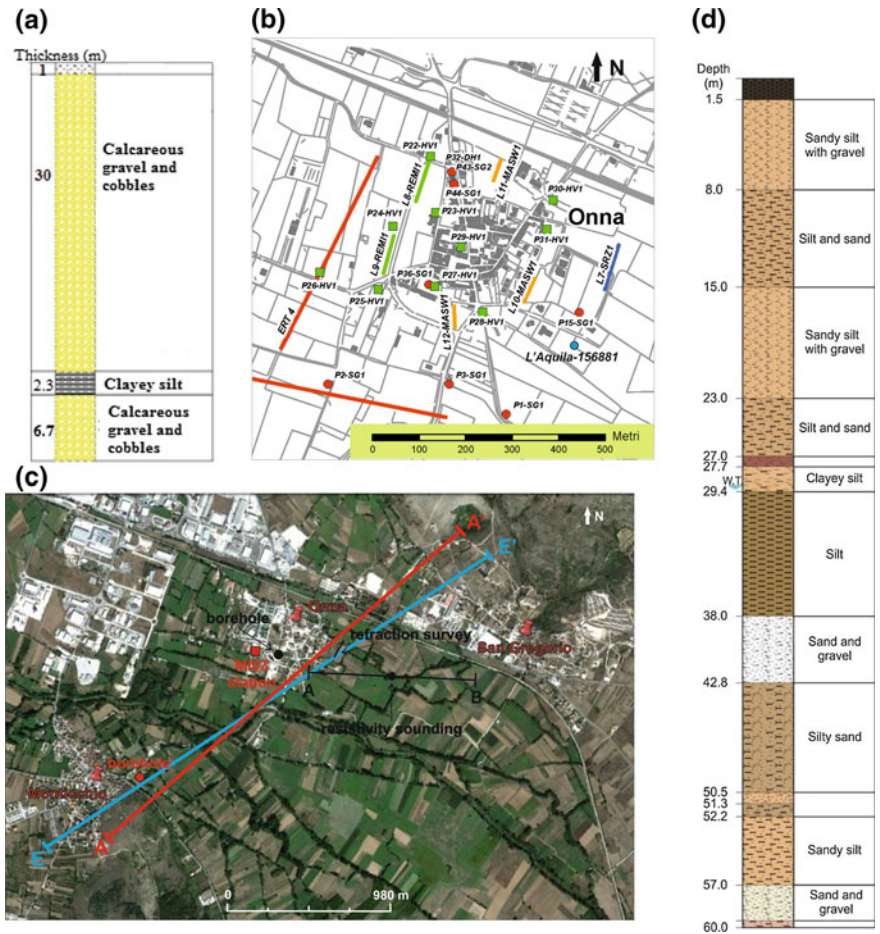


**Fig. 29** **a** Stratigraphic profile from a 40 m sounding at Monticchio site (After Monaco et al. 2009 modified). **b** Map of investigation at Onna (After Working group MS-AQ 2010 modified); boreholes (red circles); microtremors measurements (green squares); well drilled by ISPRA (blue square); electrical resistivity tomography (ERT) surveys (red lines); are refraction microtremor surveys (ReMi), (green lines); seismic refraction survey (blue line); multichannel analysis of surface waves (MASW) surveys (yellow lines). **c** Traces of two cross-sections within the Aterno River Valley at Onna site: section EE' is used for the present 2D numerical analyses; section AA' refers to the geological section. **d** Stratigraphic succession observed by the writing authors along the 60 m borehole performed nearby MIO3 station at Onna city (borehole in black in Fig. 29c)

1000 m/s along the range depths 40–50 m. Accordingly, the borehole shows the stiffer lithologies up to 57 m and up to 60 m the carbonate clasts and sand are found again. Hence, 40 m can be considered a “seismic bedrock” according to the seismic soil classification of the building code.



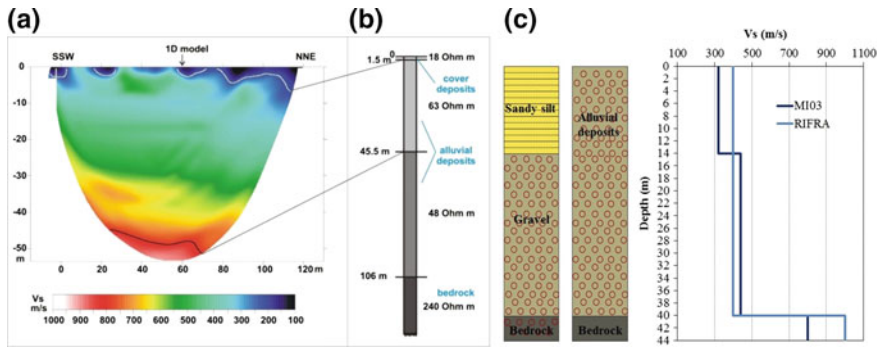


**Fig. 30** Shear waves tomographic section carried out at the Onna site (a); resistivity depth-sounding carried out at the Onna site (b); c Litho-seismic model at Onna seismic station named MI03: in red, the shear wave velocity profile measured by Working group MS-AQ (2010); in blue, the velocity profile measured by the present authors

Figure 30c shows a comparison between two seismic vertical profiles: on the left, the one measured by means of ESAC-FK method (Working group MS-AQ, 2010) under the MI03 seismic station (Fig. 30b, MI03 station in red) and, on the right, the seismic profile from seismic refraction lines performed at Onna by the writing authors (Fig. 30c). The two sites are 1 km away from each other, thus slight differences in lithological sequences can be appreciated. Nonetheless, with respect to seismic characterization of alluvial deposits, named gravels in the MI03 stratigraphy, agreement on the mean shear wave velocity of the first 40 m has been drawn. Accordingly, the new seismic vertical profile, named RIFRA, has been used for 2D numerical simulations: a mean shear wave velocity of 400 m/s up to a 40 m depth and a seismic bedrock, with a mean value of 1000 m/s, made of gravels and conglomerates in silty lacustrine matrix (varying point to point according to the cross-section model in Fig. 26). It is worth noticing that within the Onna sector of the Aterno River Valley, the geological bedrock deepens according to a host-graben shape; thus, the deposit thickness varies from point to point. Accordingly, the model maximum depth varies from 35 to 70 m from the center of the valley towards San Gregorio. Such seismic model of the near-surface sediments fits well with the results from Di Giulio et al. (2011) and Bergamaschi et al. (2011) studies. Finally, hydrogeological investigations performed by ISPRA (<http://sgi1.isprambiente.it/GeoMapView/index.html>) have been considered. The static water level is  $-75$  m as measured at L'Aquila-156881 well (Fig. 29b). Another well drilled between Bazzano and Onna, shows the static water level at  $-87$  m (L'Aquila-156727). Phreatic groundwater was measured at  $-11$  and  $-17$  m in July 2005 in the Pliocene-Quaternary deposits. At Onna, the writing authors performed a measure of groundwater level at a piezometer located in the borehole drilled near the MIO3 station (Fig. 29d): the water level was detected at a 29 m depth. Nonetheless, due to the variable characters of the continental deposit permeability, a detailed hydrogeological study is needed to assess point by point the groundwater level in the Aterno Valley.

Hereafter, 2D numerical simulations of the Monticchio-Onna-San Gregorio cross section were performed according to the model shown in Fig. 31. The aims of this study are twofold:

1. to build adequate numerical models for simulating local seismic effects. To this end, comparisons among 1D and 2D numerical results and actual records at MI03 seismic stations (at Onna) have been addressed;
2. to try to estimate the contribution to the total amplification due to the seismic bedrock variable geometry and to the seismic impedance contrasts of soil deposits at Onna. The focus on the Onna site is strictly related to three strong aftershocks recorded at that site and available on the Itaca website. The 2D numerical model used hereafter is derived from the geological section published by Working group MS-AQ (2010), shown in Fig. 31a and modified based on geophysical investigations performed by Rainone et al. (2010) and described in this section. At the bottom of the proposed numerical model, unit 1 or gravels from Table 7 are considered as the seismic bedrock because the depth of the geological bedrock is not known. The Monticchio-Onna-SanGregorio cross-section under study is rotated with respect to the reference section. In doing this, the authors aligned the studied section with the geophone locations 4824, 4823 and 4826 (Fig. 14). It is traced in Fig. 29c.

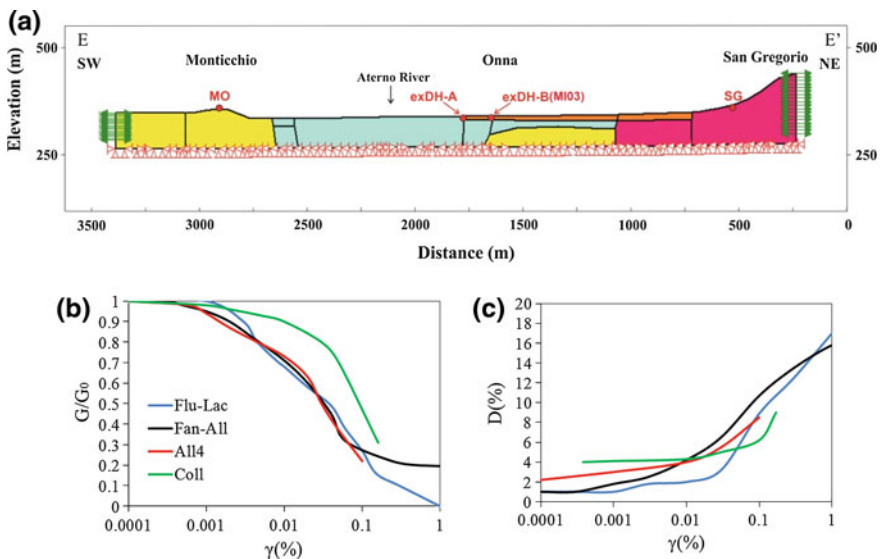


**Fig. 31** a 2D seismic model of the Onna sector of the Aterno Valley; b Normalized shear modulus reduction and c damping ratio curves with shear strain used for linear-equivalent constitutive law within the numerical analyses

**Table 7** Values of physical and mechanical properties of soil and rock units within the simulated section

Lithologic unit	Description	$\gamma$ (kN/m <sup>3</sup> )	$V_s$ (m/s)	G (MPa)	Shear modulus reduction and damping curve in Fig. 34
1 (orange)	Eluvium-colluvium deposits	18	350	200	Coll
2 (light blue)	Alternations of gravel, sand and clay	19	450	390	All4
3 (yellow)	Gravels	21	1000	2100	Fan-All
4 (fuxia)	Weathered carbonate bedrock	21	800	1300	Rock (by Idriss <sup>a</sup> )

<sup>a</sup>After Shake91 (Schnabel et al. 1991)

Dynamic numerical analyses were performed based on the soil properties at Onna (Macroarea 5) and San Gregorio (Macroarea 3) measured through several research works published during the last three years (Monaco et al. 2009; Di Giulio et al. 2011; Bergamaschi et al. 2011) and from the authors field experience at the Onna site (geophysical investigation in Fig. 29b). The equivalent linear model was used to simulate the response of all the formations; the elastic dynamic properties are reported in Table 7. Figure 31c, d shows the variation of the shear modulus reduction curves and the damping ratio curves with the shear strain measured by Compagnoni et al. (2011). For the weathered carbonate bedrock outcropping at San Gregorio, curves from literature are used: such curves are retrieved from Shake91 code (Schnabel et al. 1991). Although Working group MS-AQ (2010) reported the presence of terraced deposits of Valle Majelama Synthem superimposed on the calcareous bedrock, the authors on-site observations at the geophone locations identified only a fissured calcarenite unit. Thus a mean value of 800 m/s for shear wave velocity is used within numerical analyses (Table 7 and Fig. 31a). Moreover, according to the authors' knowledge on the hydrogeological characteristics of the Onna sector of the Aterno River Valley, the groundwater level within the numerical analysis has been considered at a 40 m depth, although locally the presence of hanging superficial groundwater can be found due to the depositional system.

The investigated section (Fig. 31a) covers 3250 m in length and 80 m in elevation; the numerical method used is the finite element implemented in QUAKE/W (Krahn 2004). Rectangular shaped elements have been used in the finite element domain discretisation. The optimum maximum size of the finite elements has been derived from the following rule, after Kuhlemeyer and Lysmer (1973):

$$l_{\max} = \frac{V_s}{7 \cdot f_{\max}} \quad (5.2)$$

where  $V_S$  is the shear wave velocity of the element material and  $f_{max}$  is the maximum frequency value of the input signal to be propagated toward the surface, which is assumed to be 20 Hz. The boundary conditions applied to lateral cut-off boundaries are nodal zero vertical displacements and nodal horizontal dampers with a viscosity coefficient,  $D_{node}$ , the values of which have been derived from the relationship:

$$D_{node} = \rho V_S \cdot L/2 \cdot 1 \tag{5.3}$$

where  $\rho$  is the density and  $V_S$  is the shear wave velocity of the material, and  $L/2$  is half the distance between the nodes times a unit distance into the section. Finally, the boundary conditions at the bottom of the model are nodal zero vertical displacements and the horizontal input time history accelerations.

The input motions considered and applied to the bottom of the model (Fig. 31a) are the time histories plotted in Fig. 24. In Fig. 32 the acceleration response spectra of these input motions are plotted according to the following naming:

1. the uniform hazard spectrum of the Italian Building code (NTC08) is named NORM;
2. the probabilistic uniform hazard spectrum with a return period of 475 years is named PROB;
3. the deterministic spectrum obtained from SP96 GMPE for a magnitude-distance pair ( $M_w = 6.7$ ,  $R_{epi} = 10$  km) is named DET.

It is worth noticing that, at the Onna seismic station (MI03) the main shock records are not available although three strong aftershocks have been recorded. In Fig. 32 acceleration spectra of the artificial input motions and the aforementioned aftershocks have been plotted together. It can be seen that the maxima spectral ordinates of these records vary from 0.1 to 0.42 g, whereas the ones of the artificial input motions range between 0.6 and 1 g. From this evidence and in order to

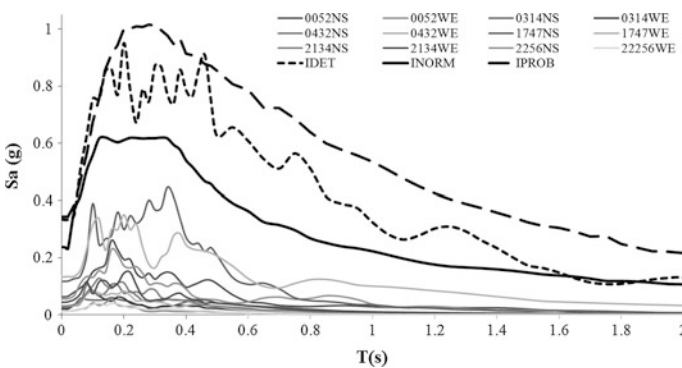


**Fig. 32** Acceleration spectra of artificial input motions simulating 6th April 2009 main shock and the strongest aftershocks recorded at Onna seismic station (MI03)

compare the calculated 1D and 2D acceleration spectra with the available records at the Onna site, the preceding three artificial inputs have been scaled at three peak acceleration values PGA: 0.05, 0.15 and 0.25 g. Then, these time histories have been deconvolved by means of 1D EERA code (Bardet et al. 2000) at the bottom of the section model, that is 70 m depth, through the gravels (reported in Table 7). The spectra of nine deconvolved input signals are reported in Fig. 33. These deconvolved acceleration spectra are all characterized by a valley at about 0.3 s, that means the fundamental resonance period of this 70 m soil column corresponds to that period, as can be easily confirmed by means of the formula:

$$T_0 = \frac{4 \cdot H}{V_s} \quad (5.4)$$

Moreover, two ranges of periods are amplified: the first one is narrow and corresponds to 0.15 s (6.7 Hz), the second one is larger varying from 0.5 to 0.75 s (1.4–2 Hz). These modifications to the artificial spectra are related to the deconvolution through the gravels, assumed as the seismic bedrock. For the purpose of this numerical study carried out along the Monticchio-Onna-San Gregorio alignment, this seismic bedrock model seems to be the most representative, provided that (1) the input motions are artificially calculated and take into account the 2009 L'Aquila earthquake main shock not recorded at the Onna seismic station and (2) accurate geotechnical and geological characterization of deep deposits is not available.

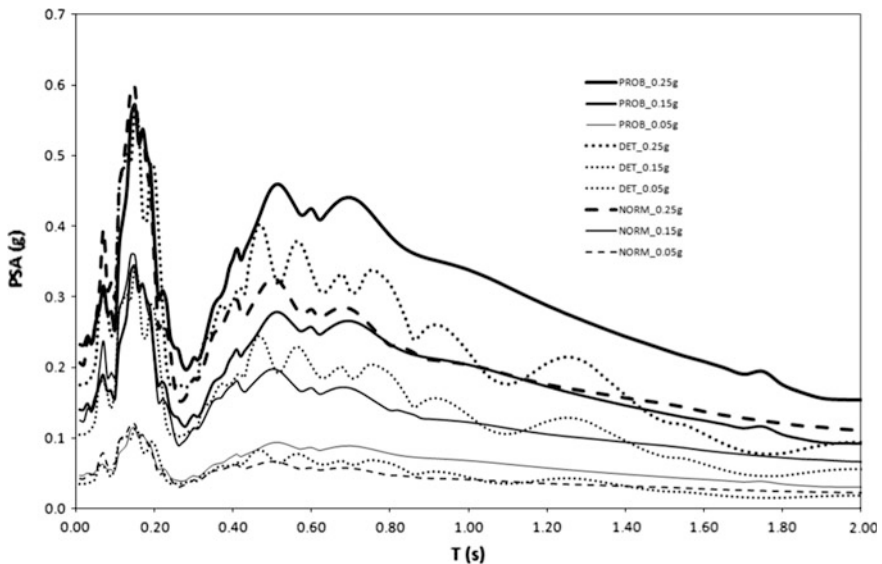


**Fig. 33** Artificial input signals called NORM, DET and PROB scaled at 0.05, 0.15 and 0.25 g and deconvolved to the bedrock depth 70 m for performing the 2D analyses within Onna sector of the Aterno Valley (Fig. 32)



Moreover, 1D and 2D numerical analysis results in terms of acceleration response spectra have been compared with three strong aftershocks recorded at the Onna seismic station (MI03): (1) on 07 April 2009 at 17:47 UTC  $M_w = 5.6$  with epicentral distance  $R_{epi} = 5.9$  km; (2) on 07 April 2009 at 21:34 UTC  $M_w = 4.6$  with epicentral distance  $R_{epi} = 10$  km; and (3) on 09 April 2009 at 00:52 UTC  $M_w = 5.4$  with epicentral distance  $R_{epi} = 20.5$  km. This seismic station corresponds to the point ExDH-B on the 2D numerical model (Fig. 31a). Another point is ExDH-A that can be representative of the Onna site, is also considered within the discussion of calculated results: at this point, the alluvial deposit deepens to 70 m whereas the surficial eluvium-colluvium deposits have constant thickness. The two points are 125 m away from each other and their differences in spectral accelerations are discussed. Figure 34a, b shows acceleration spectra calculated by means of 1D and 2D simulations, plotted together with the actual acceleration spectra recorded during the aforementioned three strong aftershocks at the Onna site (MI03). 1D Onna model for MI03 has been shown in Fig. 31c (on the left), whereas 2D point is ExDH-B. Both 1D and 2D simulations in Fig. 34a, b are related to the three artificial input motions scaled at 0.05 g. In Fig. 34a East-West record components are plotted whereas in Fig. 34b the North-South ones are shown. The studied cross section is oriented South-West and North-East, thus the two components of the records can be relevant for the comparison. As Fig. 34a shows, the 1747 record seems to be well predicted in the period range 0.05–0.3 s by the 2D simulations. Then, the valley at 0.3 s and the second amplified period, at 0.4 s are also caught. On the contrary, the “numerical” amplification from 0.4 to 0.75 s is not actually present in the aftershocks. Such difference can be due to the artificial input motions that are not built based on the Onna site response but according to the criteria summarized in Sect. 5. However, these two amplified ranges of periods are not representative for the three aftershocks under study but could be useful to predict the site response due to seismic events characterized by both larger frequency content and greater energy content. Accordingly, the authors suggest to discuss, in Fig. 34a, b, the portion of the acceleration spectra from 1D and 2D analyses that are representative for the considered records. The aim of the comparison is to point out the need of 2D simulations at Onna. In Fig. 34a the two weaker aftershocks show the same trend of the strongest one: (1) the highest acceleration peak at periods lower than 0.2 s; (2) a valley at 0.3 s and (3) smaller peaks up to 0.4 s. As can be seen, the longer the periods corresponding to the acceleration peaks the smaller the seismic event magnitude and the smaller the acceleration peaks. Such a trend is not caught by the 1D results: 1D acceleration spectra underestimate the strongest aftershocks whereas overestimate the weakest (2134 record).

Figure 34b shows that the North-South record components have different spectral acceleration trends with respect to the East-West. However, 2D results are more suitable than 1D to predict the amplifications at periods lower than 0.2 s based on 0052 and 2134 records. The North-South components seem to be influenced by a different geological setting with respect to the cross section modeled that, on the contrary, seems to be representative for the East-West components. Due to several

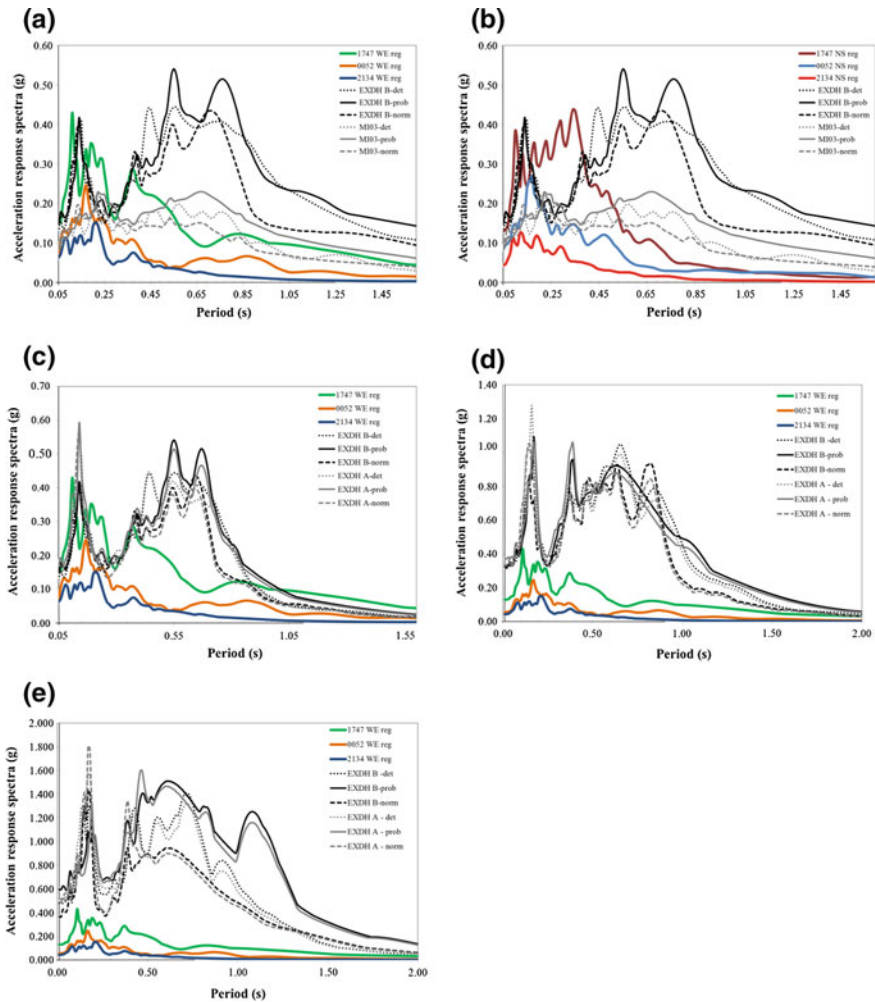


**Fig. 34** Aftershock records at MI03 (Onna seismic station), 1D (named MI03, *grey*) and 2D (named EXDH B, *black*) acceleration spectra calculated for DET, PROB and NORM artificial inputs scaled at 0.05 g, at MI03 seismic station and at the node EXDH B respectively: **a** WE record components; **b** NS record components. WE components of the aftershocks recorded at MI03 (Onna seismic station) and 2D acceleration spectra calculated at the nodes ExDH-A and ExD-B for DET, PROB and NORM artificial inputs scaled at: **c** 0.05 g, **d** 0.15 g and **e** 0.25 g

approximations in 2D numerical modeling (e.g. the 2D numerical reduction from 3D actual phenomena and the use of artificial input motions), the correspondence between the calculated and recorded acceleration spectra seem to be good for the East-West components. The 2D model used in this study enables to quantify the maximum acceleration peak and the corresponding periods both for periods lower than 0.2 s and periods up to 0.4 s. Moreover, the comparison between calculated

and recorded spectra at the Onna site confirms two assumptions proposed by the present study: the role of “seismic bedrock” played by the gravels at a 40 m depth and the need of a 2D model for a correct prediction of amplification where a basin shaped valley is detected. In the case study, the need of 2D simulations is shown at the Onna site because it is placed near the valley border. Figure 34c, e shows results from 2D simulations only. The acceleration spectra calculated at two points ExDH-A and ExDH-B on the model surface are plotted together and compared with the W-E components of the strong aftershocks recorded at the MI03 seismic station. The two points are both representative for the variable stratigraphy of the Onna city site. Thus, in order to simulate the seismic response throughout the Onna municipal territory both points are taken into account. Three artificial inputs have been considered, as in the preceding section. For calculating the acceleration spectra three PGAs have been considered. Figure 35c, e show smaller differences in the peak acceleration amplitudes at the two points for longer periods and higher differences for periods lower than 0.3 s. ExDH-A and ExDH-B are characterized by different bedrock depth. In particular, for periods lower than 0.2 s, the highest acceleration peaks are attained at ExDH-A for DET and NORM input motions. The shape of the acceleration spectra at the two points, especially at ExDH-B (with the same stratigraphy under MI03 where the aftershocks have been recorded) are in good agreement with the WE components of the strong aftershocks when the input motions are scaled at  $PGA = 0.05$  g. It well predicts the 17:47 aftershock relative to a magnitude  $M_w = 5.6$  up to 0.4 s. However, the main shock magnitude was  $M_w = 6.3$  and possibly induced higher amplifications at longer periods at the Onna city site. In order to estimate the local amplification magnitude due to both the subsurface geometry and the deposit impedance contrasts the amplification functions have been calculated at ExDH-A and ExDH-B for the input motions scaled at

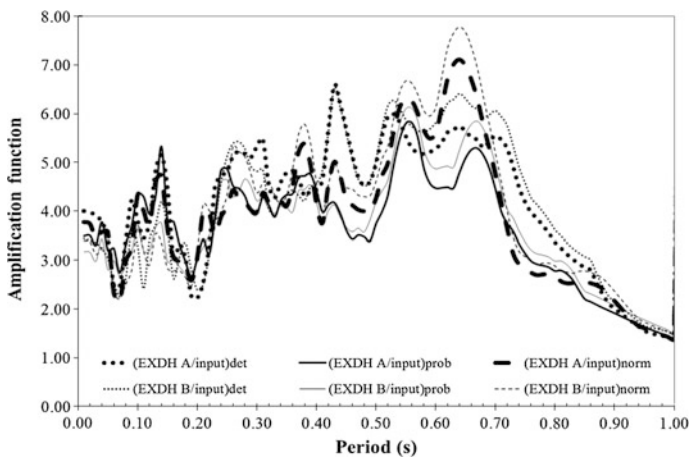


**Fig. 35** Amplification function calculated for scaled input signals at 0.05 g at Onna site (EXDH A and B)

PGA = 0.05 g. All of the amplified period ranges shown in Fig. 34c, e have been considered in order to provide suggestions on amplification functions at the Onna site taking into account a larger number of seismic records. Looking at Fig. 34d, e where input motions are scaled at PGA = 0.15 and 0.25 g respectively, a shift in amplified periods can be observed with respect to Fig. 34a: at higher PGA values, the peak at 0.12 s (8.3 Hz) is shown for PGA = 0.15 g and one between 0.1 and 0.2 s (5–10 Hz) for PGA = 0.25 g. Correspondingly, amplified higher periods vary between 0.4 and 0.8 s (1.25–2.5 s) for PGA = 0.15 g and between 0.4 and 1.2 s (0.8–2.5 Hz) for PGA = 0.25 g. The amplification functions plotted in Fig. 35 are calculated as the ratios between the numerical responses at ExDH-A and ExDH-B and input signals deconvolved to the bedrock. In the plot, the surficial amplification due to the continental deposits increases for longer periods (lower frequencies). The amplification functions vary between 2 and 5 in the period range 0.05–0.20 s (5–20 Hz), between 3.5 and 6 in the period range 0.23–0.55 s (1.8–4.3 Hz) and between 4.5 and 7.5 in the period range 0.55–0.75 s (1.3–4.3 Hz). Based on the calculated acceleration spectra, the mean amplification function at the Onna site for the period range 0.05–0.75 s is 5. This factor confirms the value suggested by Di Giulio et al. (2011) based on the analyses of spectral ratio of the strong aftershock registrations at Onna site. Whether periods lower than 0.2 s are only considered, a mean value of 3.5 can be considered for the amplification function. Moreover, at Onna site, the local amplification calculated by means of amplification function is 5, much higher than the amplification factor derived from the microzonation study at the Onna site, that is 1.8 (Fig. 36a) although it is calculated by means of a different expression (Working group MS-AQ 2010).

2D numerical results calculated at Monticchio and San Gregorio are shown in Fig. 36a. At these sites no strong motion records from the Itaca website are available, thus comparisons with velocity spectra from Sect. 4 (Figs. 12, 13 and 14) have been accomplished in terms of amplified frequencies at the three sites: Monticchio, San Gregorio and Onna. In Fig. 36a, the acceleration spectra calculated for the three artificial inputs scaled at 0.05 g at the preceding sites are plotted together. As can be seen, at the Monticchio site two amplified periods are calculated: 0.11 s (9 Hz) and 0.3 s (3.3 Hz) with the lowest acceleration ordinates with respect to San Gregorio and Onna. At San Gregorio, two amplified period ranges can be detected: 0.12–0.18 s (5.6–8.3 Hz) and 0.37–0.5 s (3–2.7 Hz). Finally, at Onna two amplified period ranges are identified: 0.14 s (7.1 Hz) and 0.55–0.67 s (1.5–1.8 Hz).

With respect to the general trend of these spectra, at Monticchio where stiffer units outcrop, the extension of the amplified period ranges is limited as well as the acceleration ordinates, whereas at the San Gregorio site the response is intermediate between Monticchio and Onna: the amplified period ranges are larger than Monticchio but narrower than Onna; on the contrary, the acceleration ordinates are higher than Monticchio but lower than Onna. All of the three sites show amplification within the period range 0.1–0.2 s. This is in agreement with the results from monitoring activity reported in Figs. 12, 13 and 14. Although the seismic events recorded can be considered weak motions, amplified frequencies higher than 5 can

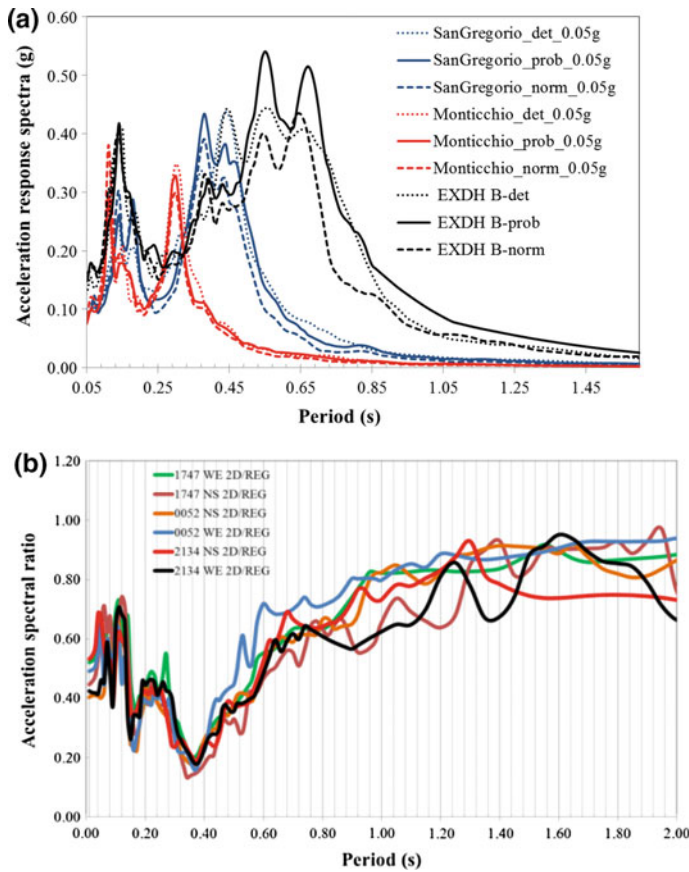


**Fig. 36** **a** Acceleration spectra calculated by means of 2D numerical analyses at Monticchio, San Gregorio and Onna for the three artificial input motions scaled at PGA = 0.05 g. **b** Spectral ratio between the aftershock records at MI03 and the corresponding deconvolved signals at 40 m depth, according to the 1D profile in Fig. 32

be detected: at Monticchio they are 8–10 Hz (0.1–0.13 s) and 2.8–3.3 Hz (0.3–0.35 s); at San Gregorio they are 8–10 Hz and 1.8–2.4 Hz; at Onna they are 7 Hz (0.14 s) and 1.3–2 Hz. These calculated responses at the three sites can help explaining the different damage levels suffered from structures. Considering the simplified expression for calculating the predominant period of a multistory building (NTC 2008):

$$T_1 = C_1 \cdot H^{3/4} \tag{5.5}$$

where H is the height of the building from the foundation level and  $C_1$  is the coefficient depending on the type of the structure: for steel structures  $C_1 = 0.085$ , for reinforced cemented structures  $C_1 = 0.075$ , whereas for other structures  $C_1 = 0.050$ .



Taking into account that at Monticchio village the buildings are prevalently masonry type with  $6 \leq H \leq 10$  m, it can be calculated that the predominant period ranges between 0.19 and 0.28 s. The amplified periods (or high frequencies) at Monticchio do not correspond to the estimated fundamental periods of the buildings. This circumstance, in addition to the lower amplification suffered by Monticchio village, can help understand the lower intensity felt here. On the contrary, at San Gregorio and at Onna, the highest peaks correspond to higher periods that likely provoked double resonance effects.

Finally, in order to address the second objective of this numerical study, that is to calculate the contribution of 2D geometry versus 1D impedance contrast on the amplification function, the strong aftershock records at Onna are deconvolved from the surface through 40 m alluvial deposits at a mean shear wave velocity of 400 m/s down to the bedrock. It is made up of gravel and conglomerate with shear wave velocity at 1000 m/s. Such a litho-seismic profile under MI03 seismic station has already been used for assessing the amplified frequency of the station (Rainone et al. 2013): here, this profile gives a possible “transfer function” for separating the geometrical amplification effects (2D effect) from those due to the soil layer impedance contrasts (1D effect). 1D analysis has been performed by EERA (Bardet et al. 2000) according to the litho-seismic profile drawn from the seismic refraction line executed by the writing authors Fig. 30c (RIFRA). The 1D deconvolution involved all of the horizontal components of the strong aftershock records at MI03 (Fig. 36b). Results are plotted in terms of acceleration spectral ratios, that are the ratio between the deconvolved signal at the bedrock and the ground records: this ratio can be regarded as the ratio between the 2D amplification effect over the total amplification on the surface.

The acceleration spectral ratios plotted in Fig. 36b show that, approximately in the period range 0.05–0.15 s (6.7–20 Hz) the geometry of the valley contributes as much as 50 % on average. As the periods increase there is a reduction in this contribution corresponding to a minor amplification effects (see Figs. 34c, d) up to 0.4 s. In the range 0.4–2 s the 2D contribution to the amplification increases: from 0.6 to 2 s it increases up to 90 %. This means that, for the soils considered, the impedance contrast plays a relevant role up to 0.15 s because it is responsible for the 50 % of the recorded amplification; for higher periods, its contribution reduces to minimum values at 2 s. These outcomes are consistent with the quite simple mean seismic profile measured over 40 m at the Onna site within the alluvial deposits and it can explain the two amplified period ranges observed: at low periods (high frequency). The sediment/bedrock impedance and the geometric amplification contribute at 50 %; on the contrary, the geometric amplification is prevalently responsible for high peaks at longer periods (lower frequency).

### 5.3 Concluding Remarks from 1D and 2D Numerical Simulations

The present section discusses some critical points raised from the great work undertaken from the Working Group MS-AQ (2010) aiming at microzoning macroareas 1 and 5 in the Aterno Valley. Results from 1D simulations performed by the writing authors at two seismic stations at L'Aquila city center and at Onna city, highlight the relevance of the local seismic effects confirmed by strong motion records of the main shock on April 6th and some strong aftershocks occurred soon after. Nonetheless, at L'Aquila city 1D simulations are able to catch the main features of the local response only if "hanging seismic bedrock" is considered. Considering the Amplification function calculated as the ratio between the output and the deconvolved input of the 1D numerical analyses, it can be noted that a 35 % amplification occurred at 0.05 s (20 Hz) and up to 25 % over the narrow period range 0.15–0.20 s (5–6.7 Hz). These values are confirmed by the records and can be used where microzoning maps do not define the amplification (Fig. 23). At Onna city, 1D simulations cannot explain the records. Thus, 2D numerical analyses have been performed along the Monticchio-Onna-San Gregorio alignment. Results in terms of acceleration response spectra have been compared with three strong aftershocks recorded at the MI03 seismic station (Onna). These numerical analyses addressed two main objectives: (1) to calculate the mean amplification at the Onna site through the amplification functions of the acceleration spectra; and (2) to assess the contribution to the local amplification of the subsurface geometry with respect to the seismic impedance contrast. The 2D numerical results, at Onna, correctly model the strongest aftershock just in the case of the input motion scaled at  $PGA = 0.05$  g. There, a mean amplification function of 5 has been calculated over the period range 0.1–0.75 s. This study suggests to use the *amplification function of the acceleration response spectra* (that is the ratio between the output and the input spectra) instead of the amplification factor for microzoning purpose: this function can be both used as a whole, whenever amplified period ranges are searched for or it could be considered by portions, whether the mean amplification values are considered in limited period ranges. Finally, the contribution of 2D geometry has been estimated at Onna site by means of deconvolving the strong aftershocks through the 1D stratigraphy at MI03: it weighs 50 % over the total amplification for periods lower than 0.4 s, whereas for higher periods it increases up to 90 %. These results contribute to shed light on the key role of subsurface geometry in local amplification effects in "near field" conditions, although limited to a few records and to the Onna site. These numerical analyses suggest that numerical models don't need to be complicated but effective on average due to the high heterogeneity and complexity of the actual subsurface settings in alluvial filled valleys.

## 6 Microzoning by Means of Ambient Noise Measurements

### 6.1 Theoretical Aspects and Limitations of Nakamura Method

Nakamura (1989) technique uses ambient noise measures to derive seismic properties of the site. The method was first introduced by Nogoshi and Igarashi (1971) based on the initial studies of Kanai and Tanaka (1961) and it is known as the “H/V method”. Among the empirical methods the H/V spectral ratios on ambient vibrations (microtremors) is probably one of the most common approach and it is actually the recommended technique to derive the natural frequency of the site in microzoning studies in Italy (ICMS 2008, 2010). The H/V method assumes that microtremors are made up of Rayleigh waves that propagate in the soft half infinite stratum of soil that is responsible of the local amplification (Fig. 37). The advantage of this method consists on separating the contribution of the source to path from the site in terms of frequency content of the signals through the ratio among recorded signal components avoiding the troublesome selection of a reference site.

Nakamura’s method is applied to four spectra in the frequency domain, that are two pairs of Horizontal ( $H_S$ ,  $H_B$ ) and Vertical ( $V_S$ ,  $V_B$ ) components related to the soft layer overlaying the rigid one according to the model in Fig. 37. In order to give some outlines of the Nakamura method, the hypotheses underneath the procedure are listed:

- Microtremors are generated by local sources;
- Surficial sources of microtremors do not affect the deep sources;
- The vertical component of the motion is not affected by the local amplification of the surficial soft layer.

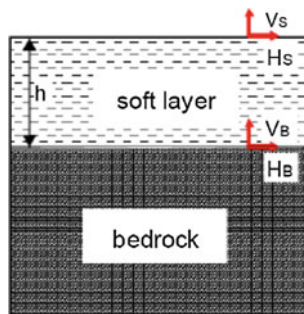


**Fig. 37** Reference model for H/V method:  $V_S$  and  $H_S$  are the vertical and horizontal components of the motion on the surficial layer;  $V_B$  and  $H_B$  are the vertical and horizontal components of the motion on the bedrock

Under these hypotheses, the ratio between the vertical components of the motion is affected by local source effects, whereas the ratio between the horizontal components of the motion is affected by both local source and amplification. Thus, multiplying the two ratios the transfer function  $S(f)$  can be calculated:

$$\frac{H_S(f)}{H_B(f)} \cdot \frac{V_S(f)}{V_B(f)} = S(f) \quad (6.1)$$

Within the hypothesis that at the bottom of the soft layer, the following expression is satisfied:

$$\frac{V_B(f)}{H_B(f)} = 1 \quad (6.2)$$

Then, the expression of the transfer function in Eq. (7) gives:

$$\frac{H_S(f)}{V_S(f)} = S(f) \quad (6.3)$$

The simplified approach that Nakamura's method relies on shows advantages and disadvantages when actually applied to the complex environments that urbanized centers represent. Thus, some guidelines have been issued from the SESAME project (Site Effects Assessment using Ambient Excitations, European Commission, no. EVG1-CT-2000-00026, Coordinator: Pierre-Yves Bard, May 1st, 2001–December 31th, 2004, Keywords: Earthquake—Site effects—Noise—Urban Area). These guidelines provide some recommendations to be taken into account when the H/V technique is used to deal with microzoning studies. The recommendations given apply basically to the case where the method is used alone on noise measures for assessing the natural frequency of sites of interest and are therefore based on a rather strict set of criteria. They are made of two parts: (1) experimental conditions and (2) criteria for reliability of results. In particular, some advices are provided when H/V technique is used within the urban centers:

- (a) Users are advised that recording near structures such as buildings, trees, etc., may influence the results: there is clear evidence that movements of structures due to the wind may introduce strong low-frequency perturbations in the ground. *Unfortunately, it is not possible to quantify the minimum distance from the structure where the influence is negligible, as this distance depends on too many external factors* (structure type, wind strength, soil type, etc.).
- (b) Avoid measuring above underground structures such as car parks, pipes, sewer lids, etc.; these structures may significantly alter the amplitude of the vertical motion.
- (c) Wind probably has the most frequent influence and we suggest avoiding measurements during windy days. Even a slight wind (approx. >5 m/s) may strongly influence the H/V results by introducing large perturbations at low

frequencies (below 1 Hz) that are not related to site effects. A consequence is that wind only perturbs low frequency sites.

- (d) Measurements during heavy rain should be avoided, while slight rain has no noticeable influence on H/V results.
- (e) Extreme temperatures should be treated with care, following the manufacturer's recommendations for the sensor and recorder; tests should be made by comparing night/day or sun/shadow measurements.
- (f) Low pressure meteorological events generally raise the low frequency content and may alter the H/V curve. If the measurements cannot be delayed until quieter weather conditions, the occurrence of such events should be noted on the measurement field sheet.

## 6.2 *H/V Ratios Measured at Macroarea 6 in the Aterno Valley*

The writing authors observed all the preceding advices and guidelines in the study presented hereafter. With the purpose of validating the Nakamura method at Villa Sant'Angelo and Tussillo site (Macroarea6), microtremor acquisitions have been performed by means of two devices:

- The Tromino, that is composed of three high-definition electrodynamic velocimeters set orthogonal to one another and put in a box. These velocimeters are characterized by a frequency range of acquisition varying between 0.1 and 256 Hz. The data are recorded in a memory card of 256 Mb with no cables inside the box;
- The DAQLink III, that is a seismometer with a 24 bit acquisition system (Seismic source Co.) and a three components geophone. This type of seismometer records continuously with a sampling window ranging from 0.0208 to 16 ms and a sampling frequency varying between 48,000 and 64.5 sample/s; the Bandwidth varies in the range 0–15 kHz and the analogic filter has a flat response up to 8000 Hz.

On January 20, 2010, 8 noise measurements through the Tromino and 4 through DAQLink have been performed nearby the points investigated at Villa Sant'Angelo and Tussillo by the National Department of Civil Protection (DPC) and Prof. Mucciarelli through the Nakamura method (Fig. 38a).

The following acquisition parameters have been used:

- Time windows longer than 30 min with sampling frequency higher than 125 Hz and sampling time lower than 8 ms;
- The transient portions of the record have been erased according to the SESAME guidelines;



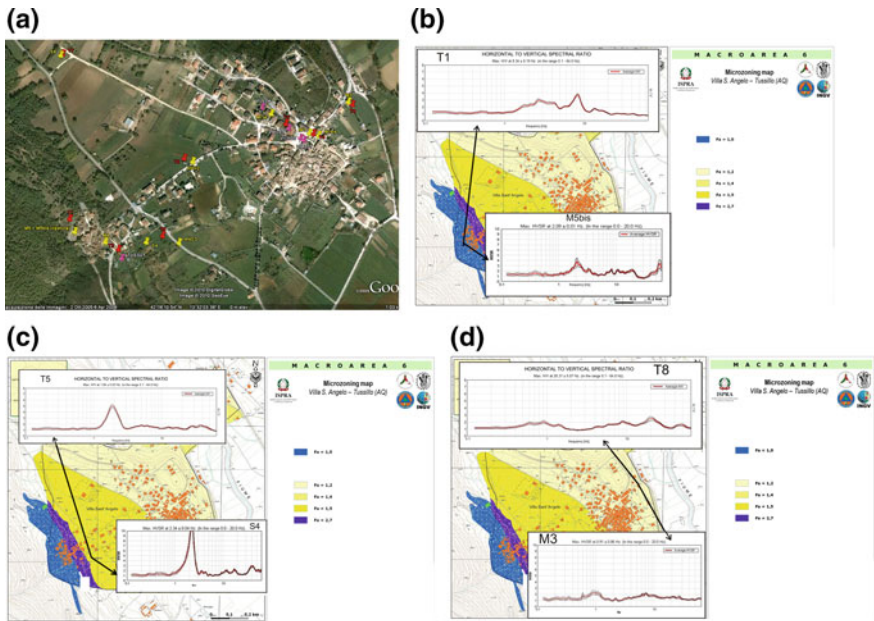


**Fig. 38** a Noise measurements locations performed at Villa Sant’Angelo-Tussillo: (in red) by the authors of this study; (in yellow) DPC; (in pink) by Prof. Mucciarelli. b H/V measurements at two neighbor points at Tussillo center: T1 (this study) and M5bis (DPC). c H/V measurements performed by the Tromino at: T5 (this study) and at S4 (DPC) under similar ground conditions. d Noise measurements recorded at Tussillo center: at T8 (this study); at M3 (DPC)

- Fast Fourier Transform has been used to calculate the H/V with the tapering step;
- The spectral smoothing has been performed by means of the Konno-Ohmachi smoothing window: where b parameter is equal to 40 (for the DaqLink records) and Triangular smoothing window (for the Tromino records)

The H/V ratios have been calculated for each sub-windows of 20 s, then the mean and the standard deviation of all ratios have been calculated and plotted (Fig. 38b, c).

Figure 38b shows the H/V measured at two neighbor points at Tussillo center: T1 (this study) and M5bis (DPC). These acquisitions have been done by the Tromino. For the present study T1 point is set on the ground (to avoid inferences with any stiff material) whereas the DPC point is set on a concrete slab. As can be noted, the two plots are different: T1 evidences two peaks at 2–3 Hz and at 8 Hz; on the contrary the M5bis shows four peaks at 2, 10–20 Hz, 40 Hz and 55 Hz. In the presence of these peaks, the operator selects the most representative one. This selection is highly subjective. With respect to the plots, from the T1 8 Hz can be taken whereas from M5bis 2 Hz should be reasonable. On the contrary, Fig. 38c shows the H/V ratios measured at two points on the same ground type at Villa Sant’Angelo center: T5 (this study) and S4 (DPC) (see Fig. 38a).

In this case, the two plots show an evident peak at 2 Hz although the peak ordinate is double at T5 with respect to S4. It could be due to the presence of Love waves that do not have vertical components contributing to the amplification of the horizontal components. Figure 38d reports the H/V ratios measured at Villa Sant’Angelo at: T8 (this study) and M3 (DPC). Both plots are almost flat and no peak frequency can be detected. Figure 39 shows the ratios measured by the Tromino at: T2 (this study), M4 (DPC) and TUSS01 (Prof. Mucciarelli). As can be seen, the three curves show similar trends but only at M4 a clear peak in the ratio can be detected at 2 Hz. The others show two smaller peaks at two frequency intervals, that are 2–3 Hz and 10–15 Hz. No clear single peak can be detected but at the M4 point (Fig. 39).

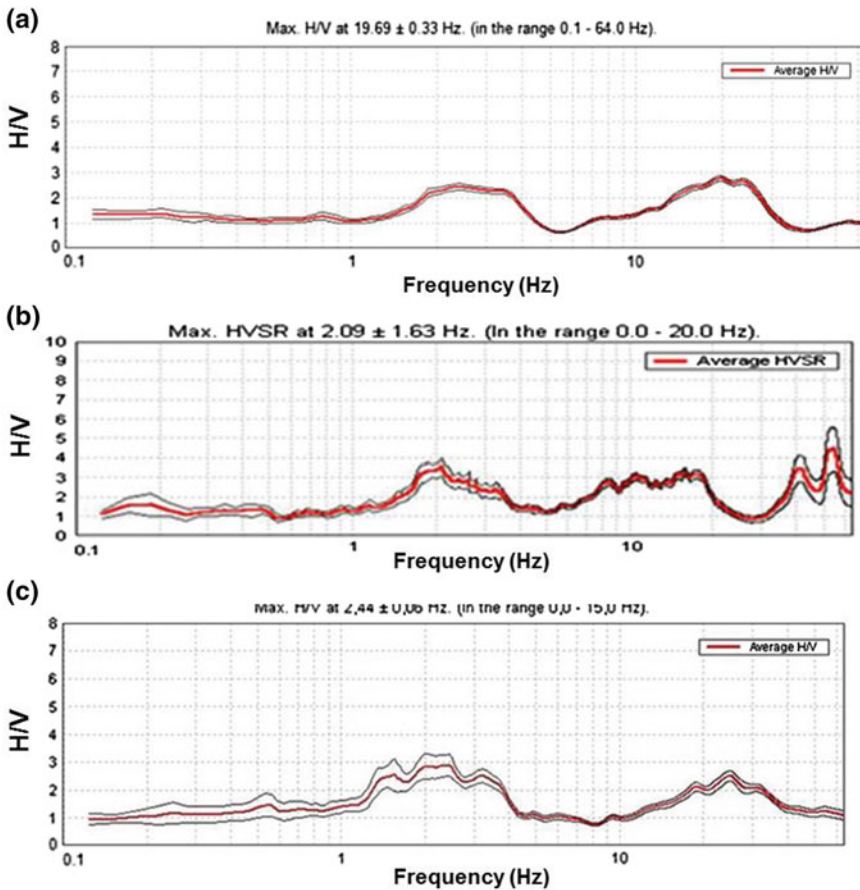
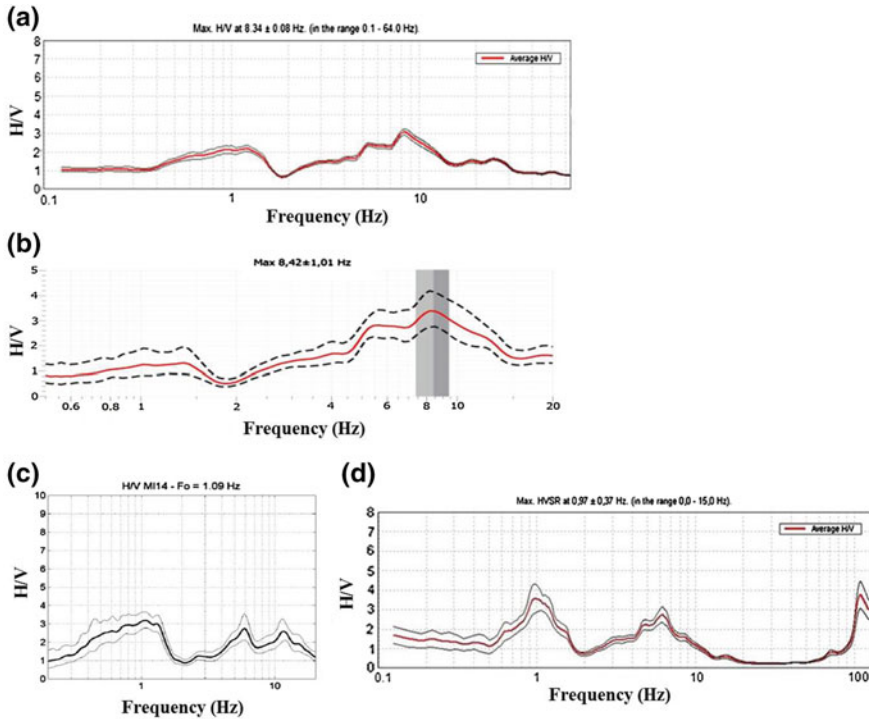


Fig. 39 H/V ratios at neighbor points at Tussillo center: a T2 (this study); b M4 (DPC); c TUSS01 (Prof. Mucciarelli)



**Fig. 40** H/V ratios at neighbor points at Villa Sant’Angelo historical center (at Municipal garden): **a** at T3 (this study) recorded by the Tromino; **b** at T3 (this study) recorded by the DAQLink; **c** at MI14 (DPC) recorded by the Tromino; **d** at VILL03 (Prof. Mucciarelli) recorded by the Tromino

Figure 40a, b show the ratios measured at T3 (this study): by the Tromino (Fig. 40a) and by the DAQLink (Fig. 40b). Thus, at the same point, H/V functions show quite similar trends and peaks: the highest is recorded at 8–9 Hz and the lowest at about 1 Hz. Comparing Fig. 40a, c, d shows that there are some differences, but peaks at 1 Hz and 6 Hz are measured at VILL03, whereas at MI14 three peaks are evident at 1, 6 and 10 Hz. Again, in these cases, different operators can derive different peak frequencies because the experimental measurements are ambiguous. Figure 41a–d compare H/V ratios measured at Villa Sant’Angelo center. In this case, the comparison between the Tromino and the DAQLink devices show similar trends and peaks. Figure 41a shows a peak at 1 Hz and 8–9 Hz, whereas the DAQLink (Fig. 41b) at 1 and 7 Hz. The measurements in Fig. 41c) shows only one peak at 1 Hz. Finally, Fig. 41d shows three peaks at 0.9–1.1 Hz, at 5–6 Hz and 8–9 Hz. No unique values from the comparisons can be drawn, indeed.

Therefore, from the comparisons of the measurements from this study at Villa Sant’Angelo and Tussillo it can be noted that the Nakamura ratio is sensitive to the site conditions and can give different predictions of the natural frequency according to the operator because often the functions show no clear peaks. Furthermore,

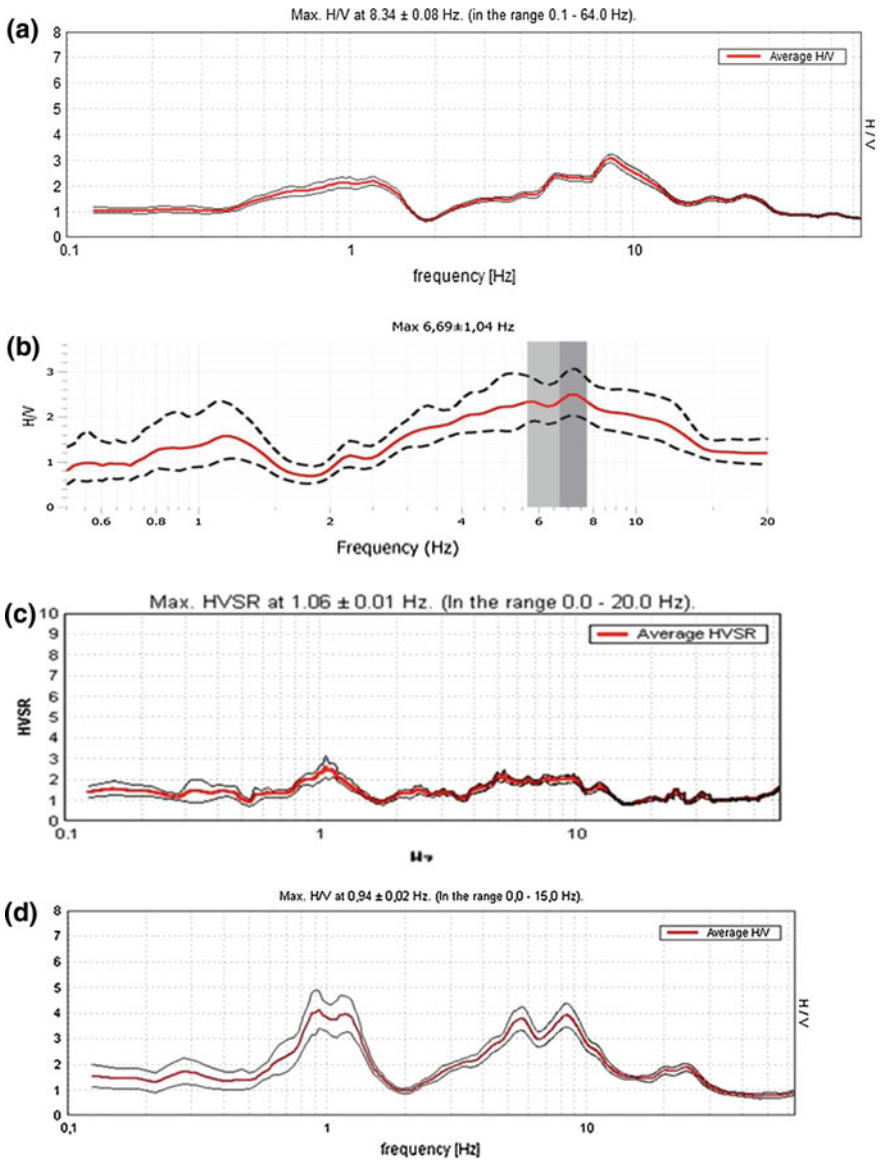


**Fig. 41** Location of noise measurements at Villa Sant’Angelo center: **a** at T4 (this study) by the Tromino device; **b** at T4 by the DAQLink device; **c** at M1 (DPC) by the Tromino device; **d** at VILL02 (Prof. Mucciarelli) by the Tromino device

measures from the two devices, Tromino and DAQLinkIII show similar ratios although variable from point to point. The noise measurements are rarely confirmed by actual records. The authors used the records from the seismic monitoring

illustrated in Sect. 5, to verify the prediction performed by the H/V ratios on the natural frequency at the site. Figure 42a, b shows the Nakamura method applied to the final portion of the records after the seismic event recorded on July 7, 2009 at 10:15 local time. As can be seen, the natural frequency derived from the peaks of the H/V ratio do not match with the peaks from the weak seismic motion records. This result comes from the comparison of weak motion and noise measurements. Through the same procedure, the authors calculated the H/V ratios by means of the final portions of the records of the main shock on April 6, 2009 at four stations: AQA, AQQ, AQM and AQV (Fig. 43). These portions are related to a few minutes after the strong motion time window. They are used to back analyze the H/V ratios from noise measurements at the seismic station points, according to D'Intinosante et al. (2007) and De Ferrari et al. (2008).

As can be pointed out, none of the peaks measured by means of the Nakamura method correspond to the peak of the strong motion records but the one calculated at AQQ station. This result cannot be predicted in advance. Moreover, the peaks from H/V correspond to higher natural frequencies in these four cases, than the ones from the weak motion records at AQQ. Finally, from the studies presented it can be drawn that Nakamura method: (1) often provides more than one peak corresponding to different natural frequencies; (2) the peaks are heavily affected especially in urban areas that can not be easily disregarded by filtering the measurements; (3) the peaks in H/V ratios are not commonly related to both weak and strong motion amplified frequencies. Thus, the use of noise measurements for microzoning activities should be discouraged especially when it is used alone and it is not validated by other geophysical testing.

### ***6.3 Concluding Remarks on Noise Measurements for Predicting the Natural Frequency of the Site***

In this last section noise measurements have been performed in order to verify: (1) their repeatability by using different acquisition devices; and (2) their ability to measure the natural frequency of the site. As shown, acquisitions repeated at the same point by the same operator through the Tromino and the Seismometer DAQLink III show similar H/V ratios. On the contrary, H/V measures acquired by means of the Tromino by different operators at different times although at neighbor points can show peaks at different frequencies or can show the same amplified frequencies but with a very different amplitude. When the noise measures are, finally, compared with the weak motion tails of actual seismic events they always show different amplified ranges of frequencies. According to the operator or the weather conditions, noise measures can provide relevant differences in amplified frequencies and cannot give reliable information on the amplification extent. Other techniques, like seismic monitoring, or the shear wave velocity measures should be preferred to estimate the natural frequency of the site. Finally, it is worth to keep in



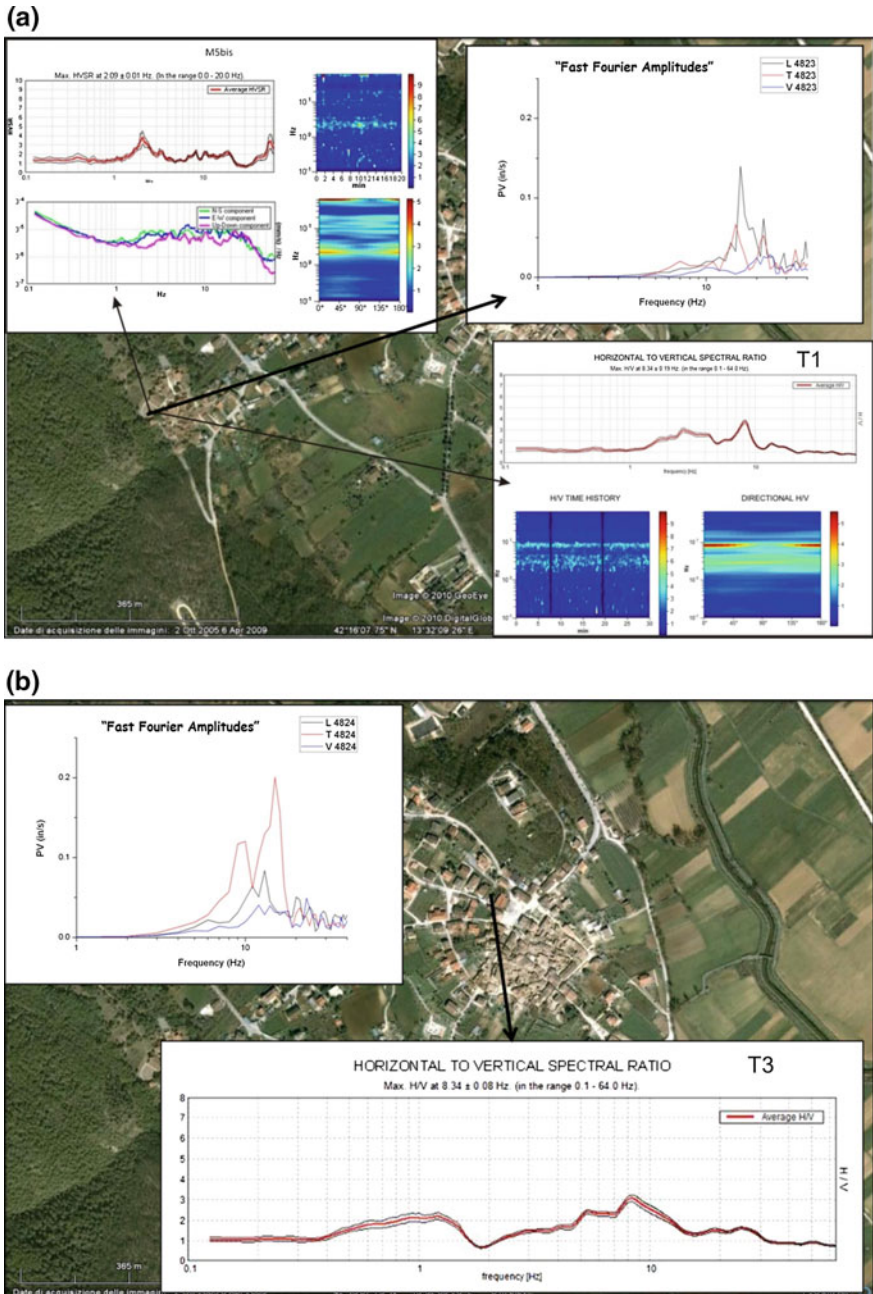
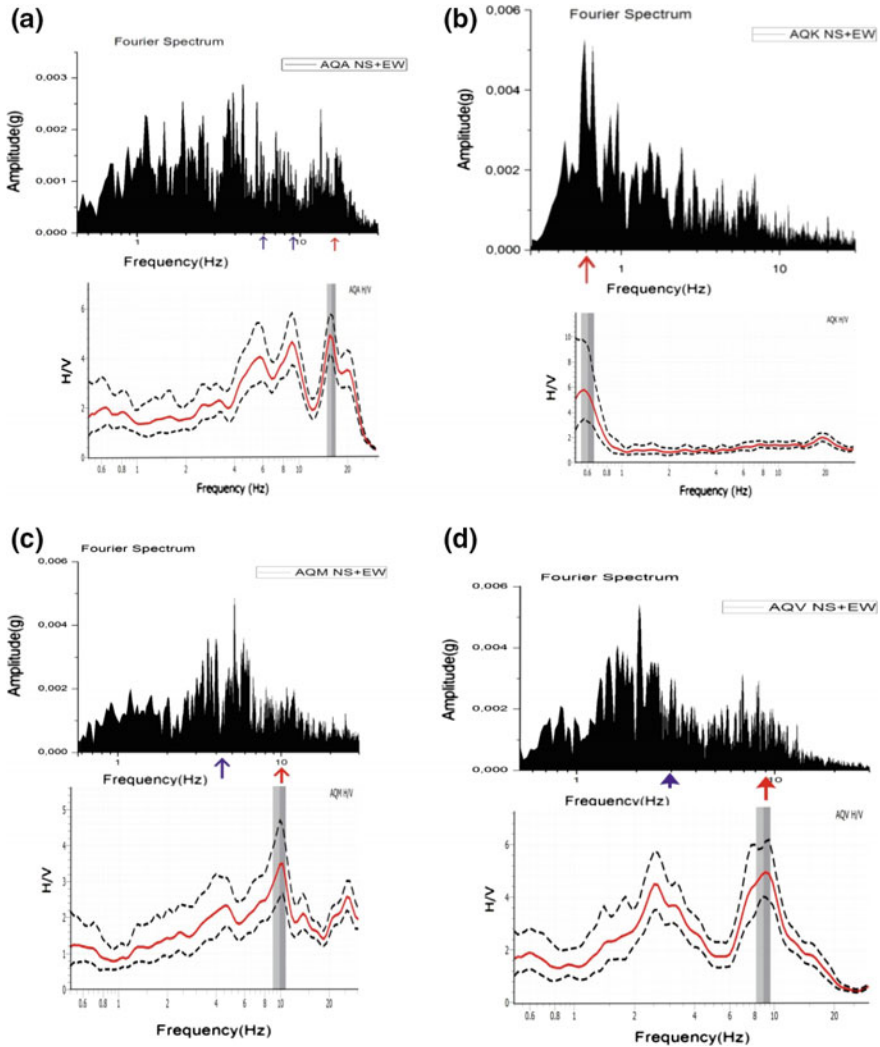


Fig. 42 Location of noise measurements from the seismic event occurred on July 7, 2009 at 10:15 local time: the noise measures are related to the final portion of the signal after the event





**Fig. 43** Pairs of Fourier spectrum and H/V ratios calculated by Nakamura’s method, related to the main shock records on April 6, 2009 at four seismic stations: **a** AQA, **b** AQK, **c** AQM, **d** AQV. The Fourier spectra is calculated from the strong motion records and the H/V ratios are calculated from the tails of the records (weak motions)

mind that soil behaviors are strain dependent. This means that their natural frequency at small strain level (microtremors) differs to a certain extent from the one at medium strain level (weak motions) and at high strain level (strong motion). Then, depending on the purpose of the natural frequency measure, different strain levels will be investigated to make the correct measure.

## References

- Amoroso, S., Del Monaco, F., Di Eusebio, F., Monaco, P., Taddei, B., Tallini, M., et al. (2010). *Campagna di indagini geologiche, geotecniche e geofisiche per lo studio della risposta sismica locale della città dell'Aquila: la stratigrafia dei sondaggi (giugno–agosto 2010)*. Report CERFIS no. 1 (in Italian).
- APAT. (2005). *Carta Geologica d'Italia, F.o 359 L'Aquila, scale 1:50,000*. APAT (Servizio Geologico d'Italia) and Regione Abruzzo. S.EL.CA, Firenze.
- Atzori, S., Hunstad, I., Chini, M., Salvi, S., Tolomei, C., Bignami, C., et al. (2009). Finite fault inversion of DIn SAR coseismic displacement of the 2009 L'Aquila earthquake (central Italy). *Geophysical Research Letters*, 36, L15305. doi:[10.1029/2009GL039293](https://doi.org/10.1029/2009GL039293)
- Bagnaia, R., D'Epifanio, A., & SylosLabini, S. (1992). Aquila and subaequan basins: An example of Quaternary evolution in central Apennines, Italy. *Quaternaria Nova*, 11, 187–209.
- Baratta, M. (1901). *I terremoti d'Italia. Saggio di storia, geografia e bibliografia sismica italiana con 136 sismocartogrammi*. Arnaldo Forni editore.
- Bardet, J. P., Ichii, K., & Lin, C. H. (2000). *EERA: A computer program for equivalent-linear earthquake site response analyses of layered soil deposits*. University of Southern California, Department of Civil Engineering.
- Bergamaschi, F., Cultrera, G., Luzi, L., Azzara, R. M., Ameri, G., Augliera, P., et al. (2011). Evaluation of site effects in the Aterno river valley (Central Italy) from aftershocks of the 2009 L'Aquila earthquake. *Bulletin of Earthquake Engineering*, 9, 697–715.
- Bosi, C., & Bertini, T. (1970). *Geologia della Media Valle dell'Aterno*, Memorie della Società Geologica Italiana (Vol. IX, pp. 719–777) (in Italian).
- Chiarabba, C., Amato, A., Anselmi, M., Baccheschi, P., Bianchi, I., Cattaneo, M., et al. (2009). The 2009 L'Aquila (central Italy) Mw 6.3 earthquake: main shock and aftershocks. *Geophysical Research Letters*, 36, L18308. doi:[10.1029/2009GL039627](https://doi.org/10.1029/2009GL039627)
- Ciriella, A., Piatanesi, A., Cocco, M., Tinti, E., Scognamiglio, L., Michelini, A., et al. (2009). Rupture history of the 2009 L'Aquila (Italy) earthquake from non-linear joint inversion of strong motion and GPS data. *Geophysical Research Letters*, 36, L19304. doi:[10.1029/2009GL039795](https://doi.org/10.1029/2009GL039795)
- Compagnoni, M., Pergalani, F., & Boncio, P. (2011). Microzonation study in the Paganica-San Gregorio area affected by the April 6, 2009 L'Aquila earthquake (central Italy) and implications for the reconstruction. *Bulletin of Earthquake Engineering*, 9, 181–198.
- De Ferrari, R., Ferretti, G., Spallarossa, D. (2008). Utilizzo di misure di rumore ambientale per la definizione degli effetti di sito: limiti di applicabilità della metodologia Nakamura. *Geologia Tecnica & Ambientale*, 2, 5–18, ISSN 1722-0025.
- Di Giulio, G., Marzorati, S., Bergamaschi, F., Bordoni, P., Cara, F., D'Alema, E., et al. (2011). Local variability of the ground shaking during the 2009 L'Aquila earthquake (April 6, 2009 Mw 6.3): The case study of Onna and Monticchio villages. *Bulletin of Earthquake Engineering*, 9, 783–807.
- DISS Working Group. (2009). *Database of individual seismogenic sources (DISS), Version 3.1.0: A compilation of potential sources for earthquakes larger than M 5.5. in Italy and surrounding areas*. Technical report, Istituto Nazionale di Geofisica e Vulcanologia (INGV).
- D'Intinosante, V., Ferrini, M., Eva, C., & Ferretti, G. (2007). Valutazione degli effetti di sito mediante l'utilizzo di rumore ambientale in alcuni siti ad elevata sismicità della Toscana Settentrionale (Garfagnana e Lunigiana), XII Congresso Nazionale "L'ingegneria Sismica in Italia", Pisa 10–14 giugno 2007.
- Galadini, F., Meletti, C., & Rebez, A. (Eds.). (2000). *Ricerche del GNDT nel campo della pericolosità sismica (1996–1999)*. Roma: CNR-GNDT, Gruppo Nazionale per la Difesa dai Terremoti.
- Galli, P., & Camassi, R. (2009). *Rapporto sugli effetti del terremoto aquilano del 6 aprile 2009*. Dipartimento della Protezione Civile Istituto Nazionale di Geofisica e Vulcanologia QUEST Team. [http://emidius.mi.ingv.it/DBMI08/aquilano/query\\_eq/quest.pdf](http://emidius.mi.ingv.it/DBMI08/aquilano/query_eq/quest.pdf)

- Gruppo di Lavoro, M. S. (2008). *Indirizzi e criteri per la Microzonazione sismica*. Roma: Conferenza delle Regioni e delle Province autonome—Dipartimento della protezione civile.
- Guidoboni, E., & Ferrari, G. (2000). Historical variables of seismic effects: Economic levels, demographic scales and building techniques. *Annali di Geofisica*, 43(4), 687–705.
- Guidoboni, E. (2006). Libro di diversi terremoti, Edizione Nazionale delle Opere di Pirro Ligorio. Edizione critica, Introduzione e Apparato storico a cura di E. Guidoboni, Roma, Editore De Luca (p. 260).
- Guidoboni E., & Comastri A. (2005). *Catalogue of earthquakes and tsunamis in the Mediterranean areas from the 11th century to the 15th century* (1037 pp). Bologna: INGV-SGA.
- Guidoboni, E., Ferrari, G., Mariotti D., Comastri, A., Valensise G., & Tarabusi, G. (2007). *CFTI4Med: Catalogue of strong earthquakes in Italy from 461 BC to 2000 and in the Mediterranean area, from 760 BC to 1500, an advanced laboratory of historical seismology*. <http://storing.ingv.it/cfti4med/>
- Guidoboni, E., Valensise, G. (2011). Il peso economico e sociale dei disastri sismici in Italia negli ultimi 150 anni (1861–2001) ([www.buponline.com](http://www.buponline.com)), INGV, Centro Euro-Mediterraneo di documentazione, Una storia Fuori dai manuali, BononiaUniversity Press.
- Guidoboni, E. (2013). *Un'altra storia: terremoti e ricostruzioni in Italia*. Centro EEDIS—Centro Euro-Mediterraneo di documentazione, 6 Dicembre, Rovereto.
- INGV—Istituto Nazionale di Geofisica e Vulcanologia. (2009). *Measurement and modeling of co-seismic deformation during the L'Aquila earthquake. Preliminary results*. Synthetic report of the activities of ASI-SIGRIS personnel and Earthquake Remote Sensing Group of the Remote Sensing Laboratory, National Earthquake Center, INGV, Rome.
- Kanai K. & Tanaka T. (1961). *On Microtremor VIII*, Bull.Earthq. Res. Inst., Tokyo University, vol.39, pp.97–114.
- Krahn J. (2004). *Dynamic modeling with quake/W*. Geo-Slope International Ltd.
- Kuhlemeyer, L., & Lysmer, J. (1973). Finite element method accuracy for wave propagation problems. *Journal of Soil Mechanics and Foundations Division*, 99, 421–427.
- Lanzo, G., Di Capua, G., Kayen, R. E., Kieffer, D. S., Button, E., Biscontin, G., et al. (2011). *The Aterno valley strong-motion array: seismic characterization and determination of subsoil model*. *Bulletin of Earthquake Engineering*, 9, 1855–1875.
- Lanzo, G., Di Capua, G., Kayen, R. E., Kieffer, D. S., Button, E., Biscontin, G., et al. (2010). Seismological and geotechnical aspects of the Mw = 6.3 l'Aquila earthquake in central Italy on 6 April 2009. *International Journal of Geoenvironment Case Histories*, 1(4), 206–339.
- Marcellini A. (coord). (1999). *Rapporto Progetto UMSEG. GNDT*. <http://it.scribd.com/doc/183624479/criteri-per-microzonazione-sismicaMS-VOLUME-2-pdf>
- Meletti C. and Valensise G. - Gruppo di Lavoro MPS (2004). *Redazione della mappa di pericolosità sismica prevista dall'Ordinanza PCM3274. Zonazione sismogenetica ZS9–App. 2 al rapporto conclusivo*.
- Milana, G., Azzara, R., Bertrand, E., Bordoni, P., Cara, F., Cogliano, R., et al. (2011). The contribution of seismic data in microzonation studies for downtown L'Aquila. *Bulletin of Earthquake Engineering*, 9(3), 741–759.
- Monaco, P., Totani, G., Barla, G., Cavallaro, A., Costanzo, A., D'Onofrio, A., et al. (2009). Geotechnical aspects of the L'Aquila earthquake. *Proceedings of 17th International Conference on Soil Mechanics and Geotechnical Engineering, Earthquake Geotechnical Engineering Satellite Conference*, 2–3 October 2009, Alexandria, Egypt.
- Nakamura, Y. (1989). A method for dynamic characteristics estimation of subsurface using microtremor on the ground surface. *Railway Technical Research Institute, Quarterly Reports*, 30(1), 25–33.
- Nogoshi M. & Igarashi T. (1971). On the amplitude characteristics of microtremor (part 2) (in Japanese with english abstract). *Journal of seismological Society of Japan*, 24, 26–40.
- NTC08. (2008). *Norme Tecniche per le Costruzioni (DM 14 gennaio 2008)*. Gazzetta Ufficiale n. 29 del 4 febbraio 2008—Suppl. Ordinario no. 30.

- Pace, B., Albarello, D., Boncio, P., Dolce, M., Galli, P., Messina, P., et al. (2011). Predicted ground motion after the L'Aquila 2009 earthquake (Italy, Mw 6.3): Input spectra for seismic microzoning. *Bulletin of Earthquake Engineering*, doi:10.1007/s10518-010-9238-y
- Postpischl, D., Faccioli, E., & Barberi, F. (1985). *Progetto Finalizzato 'Geodinamica': Monografie Finali*. Quaderni de "La ricerca scientifica", Consiglio Nazionale delle Ricerche, Editore Consiglio Nazionale delle Ricerche.
- Rainone, M. L., Torrese, P., Pizzica, F., Greco, P., & Signanini, P. (2010). *Measurement of seismic local effects and 1D numerical modeling at selected sites affected by the 2009 seismic sequence of L'Aquila*". Keystone, Colorado: SAGEEP.
- Rainone, M. L., Signanini, P., Vessia, G., Greco, P., Di Benedetto, S. (2013). L'Aquila seismic event on 6th April 2009: site effects and critical points in microzonation activity within the Aterno Valley municipalities. *Proceedings of 7th International Conference on Case Histories in Geotechnical Engineering*, April 29–May 4, Chicago.
- Salvi, S., & Working Group. (2009). *Risultati Preliminari SAR*. INGV report (in Italian).
- Schnabel, P. B., Lysmer, J., & Seed, H. B. (1991). *SHAKE—A computer program for earthquake response analysis of horizontally layered sites*. Berkeley: University of California.
- Vessia, G., Russo, S., & Lo Presti, D. (2011). A new proposal for the evaluation of the amplification coefficient due to valley effects in the simplified local seismic response analyses. *Italian Geotechnical Journal*, 4, 51–77.
- Vessia, G., & Russo, S. (2013). Relevant features of the valley seismic response: The case study of Tuscan Northern Apennine sector. *Bulletin of Earthquake Engineering*, 11(5), 1633–1660.
- Vessia, G., Rainone, M. L., Signanini, P., Greco, P., Di Benedetto, S., & Torrese, P. (2012). Integrated Geophysical and Geotechnical seismic techniques for dynamic site characterization at urbanized centers. *8th Alexander von Humboldt International Conference, Natural Disasters, Global Change, and the Preservation of World Heritage Sites*, Cusco, Peru, 12–16 November.
- Working Group MS–AQ (2010). *Microzonazione sismica per la ricostruzione dell'area aquilana*. Regione Abruzzo—Dipartimento della Protezione Civile, L'Aquila 3 vol. and Cd-rom (in Italian).